To whom I love

UNIVERSITÀ DEGLI STUDI DI SALERNO

UNIVERSITÀ DEGLI STUDI DI SALERNO
Dipartimento di Farmacia

PhD Program
in **Drug Discovery and Development**
XXXI Cycle — Academic Year 2018/2019

PhD Thesis in

Structural investigation of gp36-MPER in membrane mimicking systems

Candidate

Ilaria Stillitano

Supervisor

Prof.ssa *Anna Maria D'Ursi*

PhD Program Coordinator: Prof. Dr. *Gianluca Sbardella*

Preface

My PhD in Drug Discovery and Development was started in November 2015 under the supervision of Prof. Anna Maria D'Ursi at the Department of Pharmacy of Salerno University.

My PhD project was focalized on the study of molecular interactions using a combined approach based on the integration of different biophysical techniques.

I focalized my attention on the Membrane Proximal External Region (MPER) of gp36 glycoprotein of Feline Immunodeficiency Virus (FIV). Full gp36-MPER and its shorter peptide fragments C8, C6a and C6b were studied in different membrane mimicking systems using different spectroscopy and microscopy techniques.

The entire work was carried out under the direct supervision of Prof. Anna Maria D'Ursi. Furthermore, to improve my knowledge on NMR, gene espression and protein purification techniques, I spent a period of research activity at the Institut de Biologie Integrative de la Cellule (I2BC) of CEA, Gif-sur-Yvette-Saclay, Paris Sud, under the supervision of Dr. Francois Xavier Theillet.

List of publications related to the scientific activity performed during the three years PhD course in Drug Discovery and Development:

1) Salvo A, Rotondo A, Mangano V, Grimaldi M, **Stillitano I**, D'Ursi AM, Dugo G, Rastrelli L. High-resolution magic angle spinning nuclear magnetic resonance (HR-MAS-NMR) as quick and direct insight of almonds. *Nat Prod Res*. 2019 Feb 21:1-7.

2) Grimaldi M, **Stillitano I**, Amodio G, Santoro A, Buonocore M, Moltedo O, Remondelli P, D'Ursi AM. Structural basis of antiviral activity of peptides from MPER of FIV gp36. *PLoS One* 2018 Sep 21;13 (9)

3) Grimaldi M, Palisi A, Rossi G, **Stillitano I**, Faiella F, Montoro P, Rodriquez M, Palladino R, Maria D'Ursi A, Romano R. Saliva of patients affected by salivary gland tumour: An NMR metabolomics analysis. *J Pharm Biomed Anal*. 2018 Oct 25; 160: 436-442

4) Iacomino G, Russo P, **Stillitano I**, Lauria F, Marena P, Ahrens W, De Luca P, Siani A. Circulating microRNAs are deregulated in overweight/obese children: Preliminary results of the I. Family study. *Genes Nutr*. 2016 Mar 21;11:7

5) Iacomino G, Marano A, **Stillitano I**, Rotondi Aufiero V, Iaquinto G, Schettino M, Masucci A, Troncone R, Auricchio S, Mazzarella G. Celiac disease: role of intestinal compartments in the mucosal immune response. *Mol Cell Biochem*. 2015 Jan;411(1-2):341-9

Table of Contents

Abstract

FIV is a lentivirus that resembles the Human Immunodeficiency Virus (HIV). The lentiviral *envelope* glycoproteins (gp41 in HIV and gp36 in FIV) mediate virus entry by interacting with specific receptors present at the cell surface. Increasing evidences suggest a common structural framework for these glycoproteins, corresponding to similar roles in virus cell fusion. During the virus entry a conformational transition occurs in the glycoproteins to form a stable six-helical bundle. In this conformational arrangement, the correct assembly with the membrane of a tryptophan (Trp) rich region named membrane proximal external region (MPER) leads to the fusion of virus *envelope* and host cell membrane. The design of molecules inhibiting the correct positioning of MPER on the membrane is currently a strategy for the design of virus entry inhibitors.

C8, a Trp-rich fragment of gp36-MPER, was identified as an antiviral compound inhibiting the entry of FIV into the host cell. C8 showed remarkable membrane binding property, inducing alteration of the phospholipid bilayer and membrane fusion. In this context, part of my PhD thesis is focused on the study of C8/lipid membrane interaction employing a multiscale approach based on spectroscopic experiments, molecular dynamics simulations and confocal microscopy imaging. Our results show that the peptide is active on zwitterionic lipid environment in which it induces a structural reorganization of the phospholipid bilayer that finally leads to the formation of membrane tubules.

The presence and the position of Trp residues in C8 are important for antiviral activity: the C8 derivative C6a, obtained by truncating the N-terminal ^{770}Trp-Glu^{771} residues, exhibits conserved antiviral activity, while the C8 derivative C6b, derived from the truncation of the C-terminal ^{776}Trp-Ile^{777}, is nearly inactive. To elucidate the structural factors that induce the different activity profiles of C6a and C6b, in spite of their similarity, in the second part of my PhD thesis I

performed the study of structural behaviour of the two peptides in membrane mimicking environments using an analytical approach very similar to that employed for C8 peptide. I analysed C6a and C6b using CD and NMR spectroscopy, and confocal microscopy imaging. These data provide evidence that common antiviral activity profiles correspond to similar membrane binding properties: actually C6a, similarly to C8, has the ability to destabilize membrane vesicles, producing complex network of membrane tubes.

Eventually, I analyzed structural behavior of the full gp36-CHR-MPER in a set of membrane models characterized by increased complexity: micelles, multilamellar vesicles and cellular vesicles. Analyses with paramagnetic probes and confocal microscopy indicate that gp36-CHR-MPER and its derivatives are active on each of the mentioned bio-membrane systems, thus indicating that their impact on the size and shape is not a biophysical artefact, but an effect of biological relevance.

1 Introduction

Human Immunodeficiency Virus (HIV) is the etiologic agent of Acquired Immunodeficiency Syndrome (AIDS). This was recognized and identified in 1981, in the USA, as a peculiar syndrome characterized by a series of infections of extreme gravity caused mainly by opportunistic microorganisms and by particular neoplastic manifestations (sarcoma of Kaposi, lymphomas), as a consequence of a serious immune system deficiency.

HIV is a pathogenic retrovirus for humans, belonging to Retroviridae family, to the genus of Lentiviruses. Its genome is made up of two RNA molecules (it is therefore a ribo-virus) that, during the replicative cycle, are not directly translated, but are retro-transcribed by an enzyme, the reverse transcriptase, in many DNA molecules (provirus), able to integrate into the genome of the host cell.

With the generic name of HIV two different types of viruses are indicated: HIV-1 and HIV-2. HIV-1 is the most widespread, responsible for the AIDS epidemic in Italy and in the rest of Europe, in USA and in Central Africa. HIV-2 is mostly present in West Africa, in South America and in the Caribbean area; it is less virulent, causes disease with a relatively more attenuated course and has a lower mortality rate.

HIV-1 and HIV-2 also differ in their genomic organization: only 40% of the HIV-1 and HIV-2 sequences are identical.

Viruses capable of infecting primates, such as HIV-1 and Simian Immunodeficiency Virus (SIV), and viruses that infect non-primates, such as the Equine Infectious Anemia Virus (EIAV) and the Feline Immunodeficiency Virus (FIV) belong to Lentiviruses. FIV have been described in domestic cat (*Felis*

catus), in puma (*Puma concolor*), in lion (*Panthera leo*) and leopard (*Panthera pardus*).[1]

Under the electron microscope, the HIV virion presents an icosahedral structure (almost spherical) and a diameter of about 100-120 nm.

A careful analysis using an electron microscope allows identifying three main components: the *envelope* (pericapside), the matrix (capside) and the core (nucleocapside). The *envelope* surrounds the virus externally and consists of a double phospholipidic layer deriving from the cytoplasmic membrane of the host cell.[2] The *envelope* is surrounded by viral glycoproteins, gp120 (SU), a surface protein with antireceptor function, and gp41 (TM), a transmembrane protein with fusogenic activity, both derived from proteolytic cleavage of gp160 (product of viral gene *env*) and both involved in the virus-host cell interaction. gp41 participates more directly in the fusion process of the virus with the host cell and is placed under the gp120, folded towards the hydrophobic layer of the phospholipid membrane. The function of these proteins is to help the virus to recognize, bind and penetrate host cells.

The *envelope* surface has approximately 72 protuberances with triangular symmetry (peplomers or *spikes*); each peplomer consists of 4 heterodimers containing a molecule SU that is anchored with the -COOH portion at the N-terminal of TM protein. In addition to the virus-specific proteins, the pericapside also has proteins of cellular origin including the *Major Histocompatibility Complex* (MHC) of class II.

The pericapsidic *envelope* is followed by a layer of denser material, the matrix, 5-7 nm thick, made up of a single protein, p17 (MA), whose N-terminal is

inserted into the *envelope*. It surrounds the central part of the virus, the nucleus, contributing to the structural stability of the viral particle. The formation of the mature capside involves the proteolytic cleavage of *gag* gene initial product (p55) in the structural proteins p24, p17 and p15. Finally, there is the *core*, or nucleocapside, which has a cylindrical structure consisting of the protein 24 (p24). It contains components necessary for virus replication such as the genome, tRNA molecules necessary for the initiation of replication, non-structural proteins and *pol* gene products.

1.1 FIV

FIV belongs to the *Retroviridae* family, genus Lentivirus, and was first isolated in California in 1987.[3] It is a Lentivirus that infects domestic cats; it is not transmissible to humans and shares many biological and physio-pathogenic characteristics with HIV. Despite the enormous progress made in this field, a cure or vaccine active against HIV is not yet available[4] thus the identification of an adequate animal model is fundamental to improve the knowledge about this pathogen. Among various available models, FIV and its natural host, the domestic cat, are particularly suitable. In fact, despite the phylogenetic distance with HIV-1, there is similarity in the genomic organization, in the morphological structure, in the biological properties and in the persistence of infection in the natural host.[5]

FIV is widespread throughout the world and transmission occurs mainly through bite wounds and is frequent among male cats who live outdoors or who can leave their homes. The virus is not characterized by a high contagiousness and infection; in nature occurs with three-four clinical stages that are different from each other for symptomatology, duration and compromise of the immune system.

The first stage of the disease has an incubation period of about one month; it generates fever, lethargy and a more or less pronounced enlargement of the lymphnodes and can last weeks or even months. After this first clinical phase, cats become symptomatic carriers entering the latency phase for a very long variable period (even 3 years) without showing any clinical symptoms, but at the same time have a progressive decline of the immune defenses. As in HIV, FIV infects $CD4^+$ T cells and FIV-infected cats show a marked reduction in immune defenses and thus become vulnerable to other pathogens. The terminal stage of pathology is characterized by a rapid decay of the cat general conditions that will lead him to death. Similar to HIV and other lentiviruses, the surface glycoprotein of FIV gp45 (analog of gp120 of HIV) and the transmembrane glycoprotein gp36 (analog of gp41 of HIV), encoded by the *env* gene, play a crucial role in the early stages necessary for the virus to enter into the cell. These are considered a primary target for the immune response.

The discovery of FIV as an etiologic agent of a syndrome similar to that caused by HIV-1 in humans has from the beginning made clear the potential of this Lentivirus as a model for studying AIDS.[6] Because HIV-1 does not replicate in non-human cells, it has become necessary to use Lentivirus-animal host models to study the infection *in vivo* for the analysis of aspects related to the biology of the virus in order to develop possible therapeutic strategies and vaccine. Despite none of the animal models available represents the exact counterpart of HIV-1 infection in humans, the FIV/domestic cat system has many advantages that make it suitable for this type of study.

Other similarities of this virus with the human one include the replicative cycle, the in *vitro* cytopathic effect and the tropism for macrophages and T lymphocytes. For these reasons, FIV has been and continues to be studied to

investigate specific aspects relative to lentiviral pathogenesis and to develop antiviral drugs and therapies.

Concerning this last point, FIV has been used successfully for the development of ex *vivo* active protease inhibitors against FIV, HIV-1 and SIV.[5] FIV/cat model is also particularly attractive in the development of vaccination strategies against HIV-1. In this regard, a model advantage is that FIV, like HIV-1, has several viral subtypes, a characteristic that allows to test the effectiveness of vaccines against heterologous challenges.[7] In addition, FIV is a good model for developing safe vector systems to transduce specific cells into different organs and tissues.[8] Finally, other interesting aspects of FIV are its species specificity that reduces the risk of infection for laboratory workers who manipulate this virus and the low costs of purchase and management of animals.

1.2 Viral surface glycoproteins: gp41 and gp36

1.2.1 gp41 structure

As previously reported, the surface glycoprotein of FIV, gp45, is analogous to gp120 of HIV, and gp36, transmembrane glycoprotein is analogous to gp41 of HIV. These glycoproteins play a crucial role in the early stages necessary for the virus to enter into the cell and are considered a primary target for the immune response and for the design of anti-FIV therapeutics.[9-11]

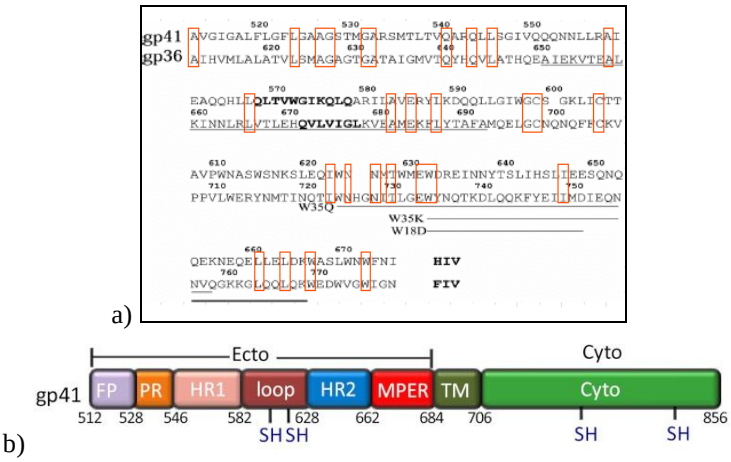

Figure 1. a) Sequence alignment between gp41 (HIV) and gp36 (FIV) performed with the CLUSTALW algorithm. b) Schematic representation of HIV gp41. The different regions are specified with abbreviations: Ecto (*ectodomain)*; FP (*fusion peptide*); FP-PR (*Fusion Peptide Proximal Region*); HR1 (*Heptad Region 1 or N heptad region*); HR2 (*Heptad Region 2 or C heptad region*); MPER (*Membrane Proximal External Region*); TM (*transmembrane region*); Cyto (*cytoplasmatic tail*).

Sequences alignment of gp41 and gp36 shows (Figure 1a) high degree of homology, with a common structural architecture that is organized as follows (Figure 1b):

- Fusion peptide (FP), a hydrophobic region rich in glycine residue, corresponding to the first 15 aa, followed by the proximal region (PR). These regions are involved in the destabilization of cell membranes.
- *Heptad Region 1* (HR1) or N heptad repeat (NHR), and *Heptad Region 2* (HR2) or C heptad repeat (CHR) at the C-terminal. The NHR and CHR regions tend to form α-helical coiled-coils,[12] necessary for fusion process of the virus with the host cell.

- Hydrophobic loop of 25-30 residues containing two cysteines forming a disulfide bridge.
- Transmembrane domain (TM), consisting of 22 amino acids, widely conserved region.
- Cytoplasmic domain (CP), consisting of about 150 amino acids endowed with important *in vivo* functions.
- Membrane proximal external region (MPER), located between the CHR and TM domain, rich in Trp residues. MPER favors the adhesion of the glycoproteins to the lipid membranes.

1.2.2 Role of gp41 in the fusion process

Interaction of gp45 (gp120 in HIV) with CD4 receptor and CXCR4, a chemokine co-receptor, causes gp36 (gp41 in HIV) conformational transition from a native state, through an intermediate pre-melting state, to an active fusion state (Figure 2).

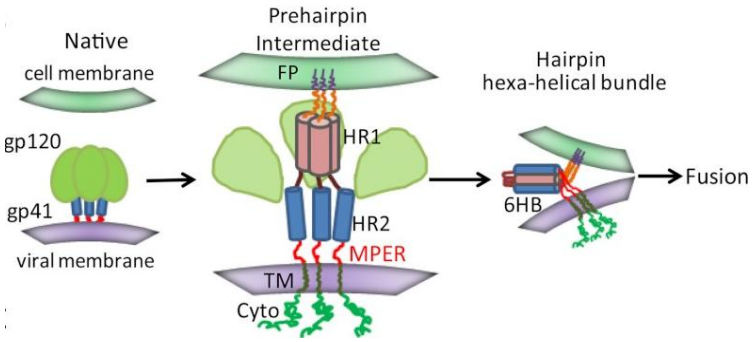

Figure 2. Schematic representation of the fusion process mediated by gp41.

In the native state, gp41 and gp120 are associated with each other so that the fusion peptide is hidden inside the *envelope*. In the pre-fusion or intermediate state, the gp41 N-terminal appears as a trimeric coiled-coil of parallel helix; the amino-terminal hydrophobic fusion peptide, placed at the top of the N-peptide coil of ectodomain, is inserted into the target cell membrane and exposes the NHR and CHR regions, thus starting the fusion process; the C-peptide region, instead, is anchored to the viral membrane by a transmembrane segment.

In the fusion state, NHR and CHR regions form a six-helical bundle (also called hairpin structure) known as the "trimeric core of antiparallel heterodimers" of the gp41 ectodomain or "hairpin trimer".

This conformational state is essential for the viral and cellular membranes to come in close proximity, ending with the release of nucleocapsid in the cytoplasm.[12, 13]

1.2.3 MPER region

MPER, acronym of membrane proximal external region, is a ~24-residue hydrophobic region (residues 660–683), immediately preceding the transmembrane domain (TM) and is one of the most conserved regions in lentivirus glycoproteins.[14-16]

MPER is rich in aromatic, particularly Trp, residues and shows a marked tendency to remain permanently at membrane interface inducing the destabilization of the target cell double layer structure. Many studies have shown that deletion or substitution of this region changes the fusogenic effects of viral glycoproteins and inhibits the virus entry into the host cell.[17] In fact, mutations of the first three Trp (Trp^{666}, Trp^{670}, Trp^{672}) are sufficient to prevent viral fusion.

It has been proposed that the MPER action at membrane interface occurs

through the formation of membranous projections rich in cholesterol (Chol) and sphingomyelin (SM). This passage represents the main energy barrier to overcome for the beginning of the fusion between the membranes and the subsequent formation of a merging pore.[18]

Peptides deriving from MPER domain of gp41 and gp36 have been extensively studied to design anti-FIV or anti-HIV therapeutics able to inhibit the fusion of HIV or FIV with host cell membranes.[19-23]

In addition, the MPER region contains epitopes that stimulate the immune response and that can be recognized by specific monoclonal antibodies, which is the reason why these domains of gp36 and gp41 are considered important targets for the development of vaccine.[24-27]

1.3 Identification of antiviral peptide C8

1.3.1 C8: Structure Activity Relationship

Based on the data that Trp residues are highly conserved in MPER of Lentivirus,[10] a sequence mapping of gp36-MPER was done by synthesizing partially overlapping peptide sequences of gp36-MPER and testing their anti-FIV activity. Accordingly, 20-mer peptide (P59) corresponding to MPER fragment 767-787 of gp36 was identified for its remarkable anti-FIV activity. In order to define the minimum active fragment deriving from P59, a series of shorter derivatives were synthesized. Among these C8 and C6a, corresponding to $gp36^{770-777}$ and $gp36^{772-777}$, were identified as the shortest anti-FIV fragments.[19] C8, including three Trp residues typical of the highly conserved pre-TM region, proved to be a potent inhibitor of FIV penetration into the host cell.[19, 20, 22, 23, 28]

An *Ala-scan* approach to define the role of the single residues for the C8 antiviral activity showed that peptides including Ala in place of Trp^{770} have a

modest antiviral action, while those characterized by the replacement of Trp^{773} or Trp^{776} with an Ala preserve anti-FIV activity.[29] All other Ala substitutions have little or no effect (Table I).

Table I: ALA-SCAN on C8.

C8	Ac-Trp-Glu-Asp-Trp-Val-Gly-Trp-Ile-NH_2
1	Ac-**Ala**-Glu-Asp-Trp-Val-Gly-Trp-Ile-NH_2
2	Ac-Trp-**Ala**-Asp-Trp-Val-Gly-Trp-Ile-NH_2
3	Ac-Trp-Glu-**Ala**-Trp-Val-Gly-Trp-Ile-NH_2
4	Ac-Trp-Glu-Asp-**Ala**-Val-Gly-Trp-Ile-NH_2
5	Ac-Trp-Glu-Asp-Trp-**Ala** -Gly-Trp-Ile-NH_2
6	Ac-Trp-Glu-Asp-Trp-Val-**Ala** -Trp-Ile-NH_2
7	Ac-Trp-Glu-Asp-Trp-Val-Gly-**Ala**-Ile-NH_2
8	Ac-Trp-Glu-Asp-Trp-Val-Gly-Trp-**Ala**-NH_2

NMR conformational studies in DMSO/water demonstrated that the anti-viral activity is associated to the prevalence of folded compact structure with critical orientation of the Trp side chains.[19] These conformational data were confirmed by subsequent studies on the reverse peptide riC8 (Ac-^{777}D-Ile-D-Trp-Gly-D-Val-D-Trp-D-Asp-D-Glu-D-Trp^{770}-NH_2), a peptide obtained by inverting the sequence and chirality of the single amino acids.[29] The conservation of riC8 anti-FIV activity was associated to its conformational stability (Figure 3).[30]

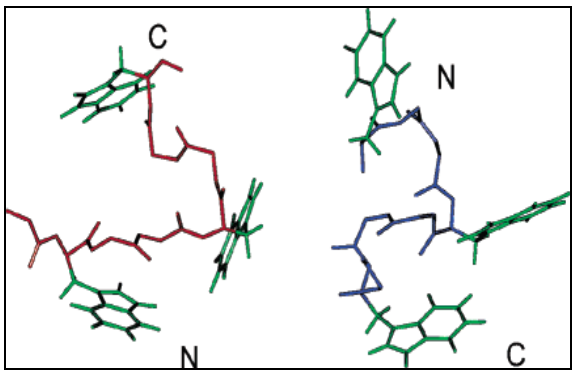

Figure 3. C8 (right) and riC8 (left) structures.

Additional SAR studies were carried out to unveil the specific role of Trp residues. Accordingly i) Trp were replaced with non proteinogenic aminoacid, by inserting aromatic moieties different than the indole ring. Trp^{770}, Trp^{773} and Trp^{776} were substituted with natural or synthetic bioisosters, such as histidine (His), phenylalanine (Phe), cyclohexyl-alanine (Cha), 1-naphthyl alanine (1-Nal), 2-naphthyl alanine (2Nal), pyridyl-alanine (Pal), benzothienyl-alanine (Bta), and biphenyl-alanine (Bip) (Table II). ii) the aminoacid spacers present in C8 were replaced by methylene chains to understand the importance the single spacers in the C8 activity. To this end alkyl spacers were used, such as 5-amino pentanoic acid (Ape), β-alanine and 8-amino octanoic acid.[31] In particular, to prove that two residues length represents an optimal distance between Trp residues to conserve anti-FIV activity, peptidomimetic was synthesized, in which the three Trp were substituted with naphtyl moieties, and the residues connecting Trp were replaced by Ape linker.[31] In addition to distance, flexibility, hydrophobicity, steric encumbrance and the different orientation of the Trp side chains, responsible for the interaction with the molecular target, proved to play an important role (Table III).

Table II: C8 analogues presenting Trp substitution.

Peptide	Sequence	IC_{50} (µg/ml)[2]
AC108	Ac-**Phe**-Glu-Asp-**Phe**-Val-Gly-**Phe**-Ile-NH_2	0.50 ± 0.06
AC112	Ac-**His**-Glu-Asp-**His**-Val-Gly-**His**-Ile-NH_2	1.80 ± 0.10
AC113	Ac-**Pal**-Glu-Asp-**Pal**-Val-Gly-**Pal**-Ile-NH_2	0.53 ± 0.23
AC114	Ac-**Bta**-Glu-Asp-**Bta**-Val-Gly-**Bta**-Ile-NH_2	0.63 ± 0.15
AC99	Ac-**Bip**-Glu-Asp-**Bip**-Val-Gly-**Bip**-Ile-NH_2	> 50
AC110	Ac-**Cha**-Glu-Asp-**Cha**-Val-Gly-**Cha**-Ile-NH_2	0.91 ± 0.21
AC98	Ac-**Nal1**-Glu-Asp-**Nal1**-Val-Gly-**Nal1**-Ile-NH_2	0.32 ± 0.11
AC109	Ac-**Nal2**-Glu-Asp-**Nal2**-Val-Gly-**Nal2**-Ile-NH_2	0.11 ± 0.10
AC111	Ac-**Nal2**-Ape-**Nal2**-Ape-**Nal2**-Ile-NH_2	0.33 ± 0.11

Table III: C8 analogs synthesized with spacers.

Peptide	Sequence	IC_{50} (µg/ml)[2]
C8	Ac-Trp-Glu-Asp-Trp-Val-Gly-Trp-Ile-NH_2	0.25 ± 0.13
AC84	Ac-**Trp**-Glu-Asp-**Trp**-Ape-**Trp**-Ile-NH_2	1.04 ± 0.83
AC86	Ac-**Trp**-Ape-**Trp**-Val-Gly-**Trp**-Ile-NH_2	1.01 ± 0.71
AC83	Ac-**Trp**-Ape-**Trp**-Ape-**Trp**-Ile-NH_2	0.32 ± 0.10
AC85	Ac-Lys-**Trp**-Ape-**Trp**-Ape-**Trp**-Ile-NH_2	1.61 ± 0.50
AC96	Ac-Lys-**Trp**-βAla-**Trp**-βAla-**Trp**-Ile-NH_2	> 50
AC97	Ac-Lys-**Trp**-Aoc-**Trp**-Aoc-**Trp**-Ile-NH_2	> 50

Structure-activity relationship studies on shorter synthetic derivatives of C8 confirmed the importance of Trp residues for the antiviral activity.[32] Experiments performed to test the inhibition of the replication of primary FIV isolated in lymphoid cells showed that the fragment of C8 (C6a) (Figure 4) deriving from the truncation of the C8 N-terminal residues ^{770}Trp-Glu^{771}, had a twofold IC_{50} activity compared to C8 (C8: IC_{50} 0.06 and 0.05 µg/ml; C6a: IC_{50} 0.15 and 0.06 µg/ml on the viral strains FIV-M2 and FIV-Pet, respectively).[33] On the contrary, the fragment of C8 (C6b) deriving from the truncation of the C8 C-terminal residues ^{776}Trp-Ile^{777}was nearly inactive, with IC_{50} values for FIV-M2 and FIV-Pet > 50 µg/ml.[33]

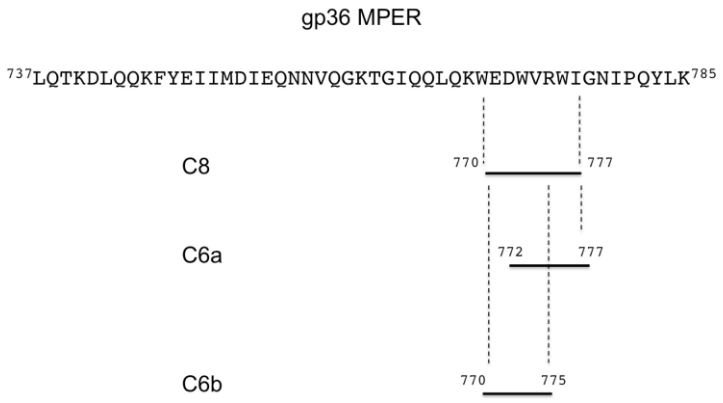

Figure 4. Graphic representation of the gp36-MPER domain of FIV coat glycoprotein. The fragments relative to C8, C6a and C6b peptide sequences are highlighted.

1.3.2 C8-lipid membrane interaction

A great deal of data showed that C8 antiviral action is related to its interaction with the host cell membrane to prevent the access of FIV.[14] To investigate the details of this mechanism, C8 was studied in several different membrane mimicking systems using different spectroscopy techniques.[19, 28-32]

Effect of C8 was examined on liposomes, formed by the zwitterionic dimyristoyl phosphatidylcholine (DMPC) and the anionic dimyristoyl phosphatidylglycerol (DMPG). Independently from the membrane charge, the peptide binds to lipid bilayers leading to membrane destabilization, fragmentation and formation of smaller aggregates.[34, 32] On palmitoyloleoyl phosphocholine (POPC) bilayers C8 was studied by spectroscopy data combined with molecular dynamics simulations (Figure 5). These studies showed that hydrogen bonds and hydrophobic interactions involving the Trp indole drive the binding of C8 with the lipid bilayer. Membrane binding induces a local decrease of the bilayer thickness, and hydration of the lipid head groups[35] culminating in the significant reorganization of the phospholipid bilayer. In membranes including SM and Chol, the type and the extent of such membrane reorganization depend on the membrane composition.[36] SM and Chol components tend to laterally segregate from glycerophospholipids, forming ordered domains, named "lipid rafts", which present reduced fluidity and permeability. Interaction of C8 with POPC induces clustering of lipids leading modifying the distribution of lipid rafts.

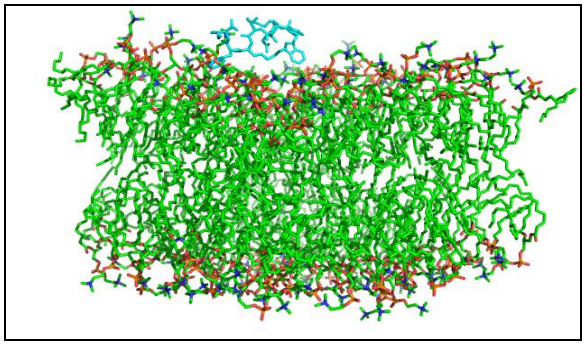

Figure 5. Interaction model of C8 peptide (in light blue) with lipid double layer surface (in green)

1.3.3 C8: NMR studies

Conformation of C8 was studied in micelle solution using NMR spectroscopy. NMR data acquired in micelle solution composed of negatively charged SDS and zwitterionic DPC, indicated that C8 undergoes a variation in its secondary structure moving from an aqueous to a membrane mimicking system obtained using micelle solutions of SDS and DPC (Figure 6).[37]

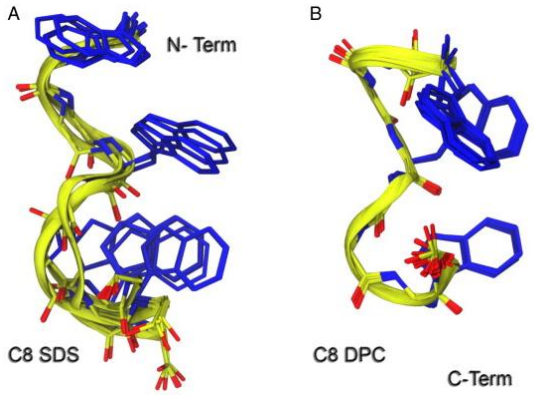

Figure 6. NMR structure of C8 peptide in micelle solutions of SDS (A) and DPC (B). The structures have been superimposed on the backbone level. The display mode was adopted using a stick and the side chains of Trp^{770}, Trp^{773} and Trp^{776} were highlighted in blue.

3D models calculated on the basis of NMR experiments in DPC micelle solutions indicate the presence of type I β-turns between Trp^{770}-Trp^{773}, Glu^{771}-Val^{774}, Val^{774}-Ile^{777}, with an ordered orientation of the amino acid side chains. Interestingly, the indole rings of Trp^{770} and Trp^{773} form a hydrophobic coating that interacts with the zwitterionic surface of DPC micelles. In SDS micelles, C8 conformation shows greater flexibility. Its hydrophobic surface is less compact and the indole rings of the Trp take different multiple orientations. C8 fluorescence spectra are imperceptibly influenced by the formation of SDS

micelles, suggesting a modest exposure of Trp residues to the SDS micelle surface.[37]

1.4 Choice of membrane mimicking system

The structural analysis of peptides endowed with strong membrane binding activity requires the choice of an experimental system that represents a valuable mimic of biological membranes.

Solution NMR spectroscopy is a suitable technique to gain high resolution structural data, but requires experimental acquisition in isotropic systems. Phospholipid bilayers represent highly biomimetic systems, but are non-isotropic systems, affecting molecular tumbling and resulting in broad NMR spectral signals.

Micelle solutions made of surfactants, at a concentration much higher than their critical micellar concentration (c.m.c.) are highly recommended for solution CD and NMR spectroscopy, as they tumble sufficiently quickly to result in high-resolution spectral lines.[38, 39] The limit of micelle solutions is that they are very simple system, extremely distant from biological membranes.

Fluorescence spectroscopy, ESR spectroscopy, microscopy imaging are possible on lipid vesicles more similar to biological membrane including, for instance, Chol and SM for the "lipid rafts" formation. Similar to micelles, the vesicles can be characterized by negative, zwitterionic or positive charge surfaces; they are usually classified according to their dimension in large, medium and small, ranging in diameters from nanometers to micrometers.

In an attempt to work on even more biomimetic systems, biophysicists and biochemists often rely on plasma membrane-derived vesicles, which are formed from cells in response to external stress.[40, 41] These vesicles are derived from the native cellular membrane, and are thus more native-like than vesicles made of

synthetic lipids. They are increasingly used in studies of lipid-lipid, lipid-protein and protein-protein interactions, and have already yielded new knowledge about lipid domains and receptor interactions in the membrane.[42-46]

The most widely used vesiculation method, developed in the 1960s, and utilizes the chemicals formaldehyde and dithiothreitol (DTT) to stress the cells and to induce an apoptosis-like response.[40, 47, 48] Vesicles can be produced with this method from a variety of mammalian cells including human embryonic kidney (HEK) 293T cells, Chinese hamster ovary (CHO) cells, A431 human epidermoid carcinoma cells, 3T3 fibroblasts, endothelial cells, a variety of other cancer cells and macrophages.[40, 43, 47-52]

In the present thesis, we used SDS and DPC micelle solution for circular dichroism (CD) and high resolution NMR conformational analysis; then we used DOPC and DOPG MLVs for ESR spectroscopy. Finally, for a macroscopic characterization, we performed confocal microscopy imaging on DOPC and DOPG MLVs and on plasma membrane-derived vesicles.

References

1. Troyer, J. L.; Pecon-Slattery, J.; Roelke, M. E.; Johnson, W.; VandeWoude, S.; Vazquez-Salat, N.; Brown, M.; Frank, L.; Woodroffe, R.; Winterbach, C. Seroprevalence and genomic divergence of circulating strains of feline immunodeficiency virus among Felidae and Hyaenidae species. *Journal of Virology* **2005,** 79, 8282-8294.

2. de Marco, A.; Müller, B.; Glass, B.; Riches, J. D.; Kräusslich, H.-G.; Briggs, J. A. Structural analysis of HIV-1 maturation using cryo-electron tomography. *PLoS pathogens* **2010,** 6, e1001215.

3. Pedersen, N. C.; Ho, E. W.; Brown, M. L.; Yamamoto, J. K. Isolation of a T-lymphotropic virus from domestic cats with an immunodeficiency-like syndrome. *Science* **1987,** 235, 790-793.

4. Montagnier, L. 25 years after HIV discovery: prospects for cure and vaccine. *Virology* **2010,** 397, 248-254.

5. Elder, J. H.; Sundstrom, M.; de Rozieres, S.; de Parseval, A.; Grant, C. K.; Lin, Y.-C. Molecular mechanisms of FIV infection. *Veterinary immunology and immunopathology* **2008,** 123, 3-13.

6. Bendinelli, M.; Pistello, M.; Lombardi, S.; Poli, A.; Garzelli, C.; Matteucci, D.; Ceccherini-Nelli, L.; Malvaldi, G.; Tozzini, F. Feline immunodeficiency virus: an interesting model for AIDS studies and an important cat pathogen. *Clinical microbiology reviews* **1995,** 8, 87-112.

7. Dunham, S. P. Lessons from the cat: development of vaccines against lentiviruses. *Veterinary immunology and immunopathology* **2006,** 112, 67-77.

8. Sauter, S. L.; Gasmi, M. FIV vector systems. *Somatic cell and molecular genetics* **2001,** 26, 99-129.

9. Giannecchini, S.; Bonci, F.; Pistello, M.; Matteucci, D.; Sichi, O.; Rovero, P.; Bendinelli, M. The membrane-proximal tryptophan-rich region in the transmembrane glycoprotein ectodomain of feline immunodeficiency virus is important for cell entry. *Virology* **2004,** 320, 156-166.

10. Salzwedel, K.; West, J. T.; Hunter, E. A conserved tryptophan-rich motif in the membrane-proximal region of the human immunodeficiency virus type 1 gp41 ectodomain is important for Env-mediated fusion and virus infectivity. *Journal of virology* **1999,** 73, 2469-2480.

11. Suárez, T.; Gallaher, W. R.; Agirre, A.; Goñi, F. M.; Nieva, J. L. Membrane interface-interacting sequences within the ectodomain of the human immunodeficiency virus type 1 envelope glycoprotein: putative role during viral fusion. *Journal of virology* **2000,** 74, 8038-8047.

12. Chambers, P.; Pringle, C. R.; Easton, A. J. Heptad repeat sequences are located adjacent to hydrophobic regions in several types of virus fusion glycoproteins. *Journal of General Virology* **1990,** 71, 3075-3080.

13. Chan, D. C.; Kim, P. S. HIV entry and its inhibition. *Cell* **1998,** 93, 681-684.

14. Frey, S. C.; Hoover, E. A.; Mullins, J. I. Feline immunodeficiency virus cell entry. *Journal of virology* **2001,** 75, 5433-5440.

15. Pancino, G.; Camoin, L.; Sonigo, P. Structural analysis of the principal immunodominant domain of the feline immunodeficiency virus transmembrane glycoprotein. *Journal of virology* **1995,** 69, 2110-2118.

16. Serres, P.-F. Molecular mimicry between the trimeric ectodomain of the transmembrane protein of immunosuppressive lentiviruses (HIV-SIV-FIV) and interleukin 2. *Comptes Rendus de l'Académie des Sciences-Series III-Sciences de la Vie* **2000,** 323, 1019-1029.

17. Muñoz-Barroso, I.; Salzwedel, K.; Hunter, E.; Blumenthal, R. Role of the membrane-proximal domain in the initial stages of human immunodeficiency virus type 1 envelope glycoprotein-mediated membrane fusion. *Journal of virology* **1999,** 73, 6089-6092.

18. Sáez-Cirión, A.; Gómara, M. a. J.; Agirre, A.; Nieva, J. L. Pre-transmembrane sequence of Ebola glycoprotein. *FEBS letters* **2003,** 533, 47-53.

19. Giannecchini, S.; Di Fenza, A.; D'Ursi, A. M.; Matteucci, D.; Rovero, P.; Bendinelli, M. Antiviral activity and conformational features of an octapeptide derived from the membrane-proximal ectodomain of the feline immunodeficiency virus transmembrane glycoprotein. *Journal of virology* **2003,** 77, 3724-3733.

20. Jiang, S.; Lin, K.; Strick, N.; Neurath, A. R. Inhibition of HIV-1 infection by a fusion domain binding peptide from the HIV-1 envelope glycoprotein GP41. *Biochemical and biophysical research communications* **1993,** 195, 533-538.

21. Jin, B.-S.; Ryu, J.-R.; Ahn, K.; Yu, Y. G. Design of a peptide inhibitor that blocks the cell fusion mediated by glycoprotein 41 of human immunodeficiency virus type 1. *AIDS research and human retroviruses* **2000,** 16, 1797-1804.

22. Kilby, J. M.; Eron, J. J. Novel therapies based on mechanisms of HIV-1 cell entry. *New England Journal of Medicine* **2003,** 348, 2228-2238.

23. Massi, C.; Indino, E.; Lami, C.; Fissi, A.; Pieroni, O.; La Rosa, C.; Esposito, F.; Galoppini, C.; Rovero, P.; Bandecchi, P. The antiviral activity of a synthetic peptide derived from the envelope SU glycoprotein of feline immunodeficiency virus maps in correspondence of an amphipathic helical segment. *Biochemical and biophysical research communications* **1998,** 246, 160-165.

24. Muster, T.; Steindl, F.; Purtscher, M.; Trkola, A.; Klima, A.; Himmler, G.; Rüker, F.; Katinger, H. A conserved neutralizing epitope on gp41 of human immunodeficiency virus type 1. *Journal of virology* **1993,** 67, 6642-6647.

25. Stiegler, G.; Kunert, R.; Purtscher, M.; Wolbank, S.; Voglauer, R.; Steindl, F.; Katinger, H. A potent cross-clade neutralizing human monoclonal antibody against a novel epitope on gp41 of human immunodeficiency virus type 1. *AIDS research and human retroviruses* **2001,** 17, 1757-1765.

26. Huang, J.; Ofek, G.; Laub, L.; Louder, M. K.; Doria-Rose, N. A.; Longo, N. S.; Imamichi, H.; Bailer, R. T.; Chakrabarti, B.; Sharma, S. K. Broad and potent neutralization of HIV-1 by a gp41-specific human antibody. *Nature* **2012,** 491, 406.

27. Williams, L. D.; Ofek, G.; Schätzle, S.; McDaniel, J. R.; Lu, X.; Nicely, N. I.; Wu, L.; Lougheed, C. S.; Bradley, T.; Louder, M. K. Potent and broad HIV-neutralizing antibodies in memory B cells and plasma. *Science immunology* **2017,** 2.

28. Wild, C. T.; Shugars, D. C.; Greenwell, T. K.; McDanal, C. B.; Matthews, T. J. Peptides corresponding to a predictive alpha-helical domain of human immunodeficiency virus type 1 gp41 are potent inhibitors of virus infection. *Proceedings of the National Academy of Sciences* **1994,** 91, 9770-9774.

29. D'Ursi, A. M.; Giannecchini, S.; Di Fenza, A.; Esposito, C.; Armenante, M. R.; Carotenuto, A.; Bendinelli, M.; Rovero, P. Retroinverso analogue of the antiviral octapeptide C8 inhibits feline immunodeficiency virus in serum. *Journal of medicinal chemistry* **2003,** 46, 1807-1810.

30. Giannecchini, S.; Alcaro, M. C.; Isola, P.; Sichi, O.; Pistello, M.; Papini, A. M.; Rovero, P.; Bendinelli, M. Feline immunodeficiency virus plasma load reduction by a retroinverso octapeptide reproducing the Trp-rich motif of the transmembrane glycoprotein. *Antiviral therapy* **2005,** 10, 671.

31. D'Ursi, A. M.; Giannecchini, S.; Esposito, C.; Alcaro, M. C.; Sichi, O.; Armenante, M. R.; Carotenuto, A.; Papini, A. M.; Bendinelli, M.; Rovero, P. Development of antiviral fusion inhibitors: short modified peptides derived from the transmembrane glycoprotein of feline immunodeficiency virus. *Chembiochem* **2006,** 7, 774-779.

32. D'Errico, G.; Vitiello, G.; D'Ursi, A. M.; Marsh, D. Interaction of short modified peptides deriving from glycoprotein gp36 of feline immunodeficiency virus with phospholipid membranes. *Eur. Biophys J.* **2009,** 38, 873-82.

33. Giannecchini, S.; Di Fenza, A.; D'Ursi, A. M.; Matteucci, D.; Rovero, P.; Bendinelli, M. Antiviral activity and conformational features of an octapeptide derived from the membrane-proximal ectodomain of the feline immunodeficiency virus transmembrane glycoprotein. *J. Virol.* **2003,** 77, 3724-33.

34. D'Errico, G.; D'Ursi, A. M.; Marsh, D. Interaction of a peptide derived from glycoprotein gp36 of feline immunodeficiency virus and its lipoylated analogue with phospholipid membranes. *Biochemistry* **2008,** 47, 5317-5327.

35. Merlino, A.; Vitiello, G.; Grimaldi, M.; Sica, F.; Busi, E.; Basosi, R.; D'Ursi, A. M.; Fragneto, G.; Paduano, L.; D'Errico, G. Destabilization of lipid membranes by a peptide derived from glycoprotein gp36 of feline immunodeficiency virus: A combined molecular dynamics/experimental study. *The Journal of Physical Chemistry B* **2011,** 116, 401-412.

36. Oliva, R.; Del Vecchio, P.; Stellato, M. I.; D'Ursi, A. M.; D'Errico, G.; Paduano, L.; Petraccone, L. A thermodynamic signature of lipid segregation in biomembranes induced by a short peptide derived from glycoprotein gp36 of feline immunodeficiency virus. *Biochimica et Biophysica Acta (BBA)-Biomembranes* **2015,** 1848, 510-517.

37. Scrima, M.; Di Marino, S.; Grimaldi, M.; Campana, F.; Vitiello, G.; Piotto, S. P.; D'Errico, G.; D'Ursi, A. M. Structural features of the C8 antiviral peptide in a membrane-mimicking environment. *Biochimica et Biophysica Acta (BBA)-Biomembranes* **2014,** 1838, 1010-1018.

38. Pandey, S.; Alcaro, M. C.; Scrima, M.; Peroni, E.; Paolini, I.; Di Marino, S.; Barbetti, F.; Carotenuto, A.; Novellino, E.; Papini, A. M.; D'Ursi, A. M.; Rovero, P. Designed glucopeptides mimetics of myelin protein epitopes as synthetic probes for the detection of autoantibodies, biomarkers of multiple sclerosis. *J Med Chem* **2012,** 55, 10437-47.

39. Mannhold, R.; Kubinyi, H.; Folkers, G.; Zerbe, O. *BioNMR in drug research*. John Wiley & Sons: 2006; Vol. 16.

40. Scott, R. E. Plasma membrane vesiculation: a new technique for isolation of plasma membranes. *Science* **1976,** 194, 743-745.

41. Del Piccolo, N.; Placone, J.; He, L.; Agudelo, S. C.; Hristova, K. Production of plasma membrane vesicles with chloride salts and their utility as a cell membrane mimetic for biophysical characterization of membrane protein interactions. *Analytical chemistry* **2012,** 84, 8650-8655.

42. Levental, I.; Grzybek, M.; Simons, K. Raft domains of variable properties and compositions in plasma membrane vesicles. *Proceedings of the National Academy of Sciences* **2011,** 108, 11411-11416.

43. Veatch, S. L.; Cicuta, P.; Sengupta, P.; Honerkamp-Smith, A.; Holowka, D.; Baird, B. Critical fluctuations in plasma membrane vesicles. *ACS chemical biology* **2008,** 3, 287-293.

44. Chen, L.; Novicky, L.; Merzlyakov, M.; Hristov, T.; Hristova, K. Measuring the energetics of membrane protein dimerization in mammalian membranes. *Journal of the American Chemical Society* **2010,** 132, 3628-3635.

45. Placone, J.; Hristova, K. Direct assessment of the effect of the Gly380Arg achondroplasia mutation on FGFR3 dimerization using quantitative imaging FRET. *PloS one* **2012,** 7, e46678.

46. Del Piccolo, N.; Placone, J.; Hristova, K. Effect of thanatophoric dysplasia type I mutations on FGFR3 dimerization. *Biophysical journal* **2015,** 108, 272-278.

47. Scott, R. E.; Maercklein, P. B. Plasma membrane vesiculation in 3T3 and SV3T3 cells. II. Factors affecting the process of vesiculation. *Journal of Cell Science* **1979,** 35, 245-252.

48. Scott, R. E.; Perkins, R.; Zschunke, M.; Hoerl, B.; Maercklein, P. Plasma membrane vesiculation in 3T3 and SV3T3 cells. I. Morphological and biochemical characterization. *Journal of Cell Science* **1979,** 35, 229-243.

49. Sarabipour, S.; Hristova, K. Glycophorin A transmembrane domain dimerization in plasma membrane vesicles derived from CHO, HEK 293T, and A431 cells. *Biochimica et Biophysica Acta (BBA)-Biomembranes* **2013,** 1828, 1829-1833.

50. Baumgart, T.; Hammond, A. T.; Sengupta, P.; Hess, S. T.; Holowka, D. A.; Baird, B. A.; Webb, W. W. Large-scale fluid/fluid phase separation of proteins and lipids in giant plasma membrane vesicles. *Proceedings of the National Academy of Sciences* **2007,** 104, 3165-3170.

51. Holowka, D.; Baird, B. Structural studies on the membrane-bound immunoglobulin E-receptor complex. 1. Characterization of large plasma membrane vesicles from rat basophilic leukemia cells and insertion of amphipathic fluorescent probes. *Biochemistry* **1983,** 22, 3466-3474.

52. Sengupta, P.; Hammond, A.; Holowka, D.; Baird, B. Structural determinants for partitioning of lipids and proteins between coexisting fluid phases in giant plasma membrane vesicles. *Biochimica et Biophysica Acta (BBA)-Biomembranes* **2008,** 1778, 20-32.

2 Investigating interaction of C8 with membrane models

2.1 Conformational analysis of C8 in DPC-SDS micelle

As reported in the previous chapter, C8 is an eight-residues peptide (WEDWVGWI) belonging to the Membrane Proximal External Region (MPER) (Figure 1) of Feline Immunodeficiency Virus (FIV) coat glycoprotein gp36. It is characterized by the presence of three equally spaced Trp residues and exerts antiviral activity by inhibiting the entry of FIV in host cell membrane.[1-7]

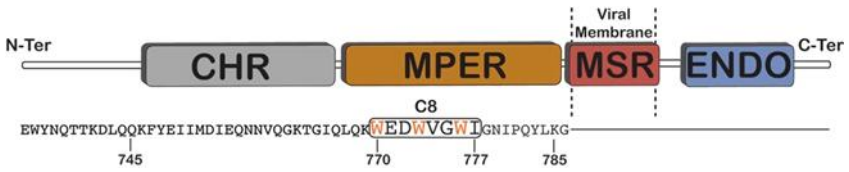

Figure 1. Graphic representation of the C-terminal domains of the feline immunodeficiency virus (FIV) coat glycoprotein gp36-CHR-MPER. The C8 peptide sequence is underlined by the black box and the three tryptophans are reported in orange.

We previously reported spectroscopic data proving that C8 is able to perturb lipid bilayer organization in several membrane mimicking systems.[1, 2, 7-11] NMR conformational analysis of C8 in micelle solution characterized by different superficial charge point to the importance of micelle charge for the secondary

structure of C8.[11] This information is of biologically paramount relevance if we consider that cell membranes are typically made by about 90% zwitterionic and 10% negatively charged phospholipids.[12]

In this framework, it is of great interest to investigate and understand how different charge conditions affect the interaction of C8 with the membrane phospholipids. To this end, part of my PhD project was aimed at investigating the interaction between C8 and differently charged membrane models, each containing a diverse ratio of zwitterionic and negatively charged phospholipids. My experiments based on spectroscopy and microscopy measurements are integrated with theoretical calculations.

2.1.1 CD and NMR conformational analyses

Micelle solutions are largely used as a biomimetic membrane model to study the structural features of membranotropic molecules. They are made of surfactants, such as the zwitterionic dodecylphosphocholine (DPC) and the negatively charged sodium dodecyl sulphate (SDS), at a concentration much higher than their critical micellar concentration (c.m.c.). These surfactants form spherical aggregates where the polar head groups are located on the surface, while the hydrophobic tail points to the centre.

From a technical point of view, micelle solutions are ideal membrane mimicking systems for solution circular dichroism (CD) and nuclear magnetic resonance (NMR) spectroscopy, as they tumble sufficiently quickly to result in high-resolution spectral lines.[13, 14]

Conformational analysis of C8 by CD and NMR spectroscopy was carried out in mixed micelle solutions at different zwitterionic DPC and negatively charged SDS molar ratio, that are the DPC/SDS molar ratio 90:10, 60:40, 40:60 and 10:90

(Figure 2). Quantitative analysis of CD spectra (DICHROWEB website)[15] indicates that C8 assumes non canonical turn conformations in DPC/SDS 10:90 M/M and increasing turn-helical conformations at increasing contents of zwitterionic DPC detergent.

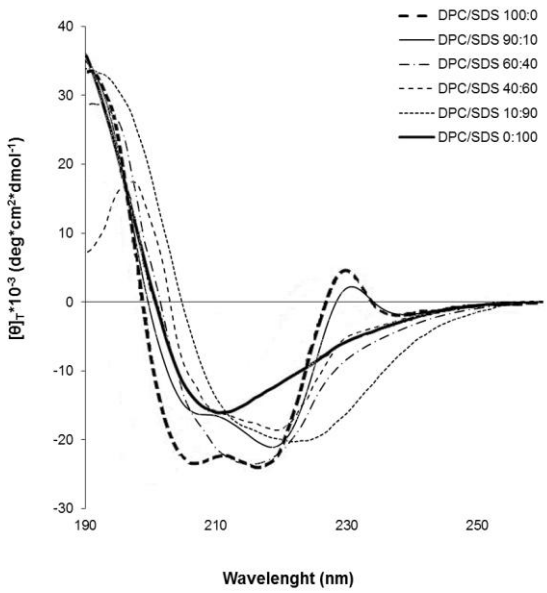

Figure 2. Normalized circular dichroism (CD) spectra of C8 in different DPC/SDS molar ratio: 100:0, 90:10, 60:40, 40:60, 10:90 and 0:100. The CD spectra were acquired using a JASCO J810 spectropolarimeter at room temperature with a cell path length of 1 mm. The measurement range spans from 190 to 260 nm.

NMR spectra of C8 in DPC/SDS micelles were recorded on a Bruker DRX-600 spectrometer. 2D COSY, TOCSY and NOESY[16-19] were recorded and analysed using SPARKY[20] software to have chemical shift assignment according to the conventional procedure of Wuthrich.[21] ^{1}H NMR experiments were recorded on C8 samples containing different proportions of DPC/SDS molar ratio: 100:0, 90:10, 60:40, 40:60, 10:90 and 0:100 (Table Ia-f).

Table Ia. ^{1}H chemical shift of C8 in DPC/SDS 100:0 M/M micelle solution.

Residue	HN	CαH	CβH	CγH	CδH	CεH	Others
Trp770	8.611	4.435	Qβ 3.308		Hδ1 7.416	Hε1 10.667 Hε3 7.637	Hη2 7.073 Hζ2 7.553 Hζ3 6.905
Glu771	9.176	3.886	Hβ2 1.999 Hβ3 1.941	Qγ 2.175			
Asp772	8.046	4.505	Hβ2 2.621 Hβ3 2.487				
Trp773	8.040	4.373	Qβ 3.415		Hδ1 7.393	Hε1 10.641 Hε3 7.548	Hη2 7.027 Hζ2 7.480 Hζ3 6.788
Val774	8.093	3.914	2.155	QQγ 0.989			
Gly775	8.176	Hα2 3.919 Hα3 3.955					
Trp776	7.507	4.449	Hβ2 3.435 Hβ3 3.387		Hδ1 7.362	Hε1 10.480 Hε3 7.559	Hη2 7.120 Hζ2 7.506 Hζ3 7.035
Ile777	7.635	3.605	1.875	Qγ12 1.544 Qγ13 1.104 Qγ2 0.957			

Table Ib. ^{1}H chemical shift of C8 in DPC/SDS 90:10 M/M micelle solution.

Residue	HN	CαH	CβH	CγH	CδH	CεH	Others
Trp770	8.513	4.388	Qβ 3.283		Hδ1 7.432	Hε1 10.522	Hη2 7.094 Hζ2 7.549 Hζ3 6.918
Glu771	8.708	3.874	Hβ2 1.911 Hβ3 1.833	Hγ2 2.148 Hγ3 2.003			
Asp772	7.992	4.487	Hβ2 2.673 Hβ3 2.555				
Trp773	7.970	4.374	Qβ 3.407		Hδ1 7.361	Hε1 10.512 Hε3 7.530	Hη2 7.030 Hζ2 7.419 Hζ3 6.805
Val774	7.952	3.894	2.152	QQγ 0.980			
Gly775	8.100	Qα 3.913					
Trp776	7.651	4.481	Qβ 3.393		Hδ1 7.340	Hε1 10.386 Hε3 7.569	Hη2 7.117 Hζ2 7.493 Hζ3 7.026
Ile777	7.556	3.644	1.834	Qγ1 1.258 Qγ2 0.907	Qδ1 0.871		

Table Ic. ^{1}H chemical shift of C8 in DPC/SDS 60:40 M/M micelle solution.

Residue	HN	CαH	CβH	CγH	CδH	CεH	Others
Trp770	8.240	4.273	Hβ2 3.219 Hβ3 3.187			Hε1 10.322	Hζ2 7.362 Hζ3 7.233
Glu771	8.209	3.773	Hβ2 1.799 Hβ3 1.682	Hγ2 2.049 Hγ3 1.885			
Asp772	7.944	4.45	Hβ2 2.722 Hβ3 2.654				
Trp773	7.840	4.346	Qβ 3.329			Hε1 10.259	Hζ2 7.449 Hζ3 7.233
Val774	7.680	3.845	2.061	Qγ1 0.906 Qγ2 0.883			
Gly775	7.974	Qα 3.839					
Trp776	7.622	4.459	Qβ 3.323			Hε1 10.222 Hε3 7.490	Hζ2 7.441 Hζ3 7.256
Ile777	7.446	3.694	1.747	Qγ1 1.334 Qγ2 0.966	Hδ11 1 0.825 Hδ12 2 0.793		

Table Id. ^{1}H chemical shift of C8 in DPC/SDS 40:60 M/M micelle solution.

Residue	HN	CαH	CβH	CγH	CδH	CεH	Others
Trp770	8.027	4.231	Hβ2 3.225 Hβ3 3.146		Hδ1 7.366	Hε1 10.155	Hη2 7.344 Hζ2 7.424 Hζ3 7.200
Glu771	7.990	3.716	Hβ2 1.756 Hβ3 1.604	Qγ 2.003			
Asp772	7.897	4.450	Qβ 2.707				
Trp773	7.793	4.385	Qβ 3.325		Hδ1 7.441	Hε1 10.083	Hη2 7.425 Hζ3 7.200
Val774	7.590	3.857	2.047	Qγ1 0.899 Qγ2 0.870			
Gly775	7.937	Qα 3.844					
Trp776	7.632	4.478	Hβ2 3.341 Hβ3 3.320		Hδ1 7.492	Hε1 10.083	Hη2 7.479 Hζ3 7.248
Ile777	7.425	3.751	1.739	Qγ1 1.292 Qγ2 0.952	Hδ11 0.812 Hδ12 0.783		

Table Ie. ^{1}H chemical shift of C8 in DPC/SDS 10:90 M/M micelle solution.

Residue	HN	CαH	CβH	CγH	CδH	CεH	Others
Trp770	7.663	4.022	Hβ2 3.075 Hβ3 2.942		Hδ1 7.143	Hε1 9.795	Hζ2 7.245 Hζ3 7.023
Glu771	8.191	3.464	Hβ2 1.376 Hβ3 1.314	Hγ2 1.628 Hγ3 1.494			
Asp772	7.601	4.254	Qβ 2.305				
Trp773	7.689	4.281	Hβ2 3.189 Hβ3 3.155		Hδ1 7.090	Hε1 9.826	Hζ2 7.245 Hζ3 7.022
Val774	7.600	3.734	1.908	Qγ1 0.796 Qγ2 0.745			
Gly775	7.786	Qα 3.659					
Trp776	7.507	4.246	Hβ2 3.204 Hβ3 3.165		Hδ1 7.235	Hε1 9.765 Hε3 7.323	Hζ2 7.294 Hζ3 7.090
Ile777	7.297	3.538	1.573	Qγ1 1.120 Qγ2 0.745	Hδ11 0.659 Hδ12 0.622		

Table If. ^{1}H chemical shift of C8 in DPC/SDS 0:100 M/M micelle solution.

Residue	HN	CαH	CβH	CγH	CδH	CεH	Others
Trp770	7.713	4.252	Hβ2 3.303 Hβ3 3.142		Hδ1 7.352	Hε1 9.917 Hε3 7.451	Hη2 7.124 Hζ2 7.407 Hζ3 6.945
Glu771	8.379	3.707	Hβ2 1.616 Hβ3 1.549	Hγ2 1.873 Hγ3 1.718			
Asp772	7.770	4.476	Qβ 2.520				
Trp773	7.884	4.581	Hβ2 3.424 Hβ3 3.367		Hδ1 7.241	Hε1 9.947 Hε3 7.576	Hη2 7.170 Hζ2 7.473 Hζ3 7.051
Val774	7.752	3.992	2.142	Qγ1 1.038 Qγ2 0.995			
Gly775	7.966	Qα 3.900					
Trp776	7.731	4.483	Hβ2 3.476 Hβ3 3.399		Hδ1 7.340	Hε1 9.887 Hε3 7.574	Hη2 7.141 Hζ2 7.492 Hζ3 6.873
Ile777	7.454	3.826	1.813	Qγ1 1.343 Qγ2 0.995	Qδ1 0.895		

NOESY spectra (as representative we show only 2 spectra, Figure 3) were the starting point to collect NOE data to calculate C8 conformation in the different DPC/SDS micelle systems. The sequential and medium range connectivities (Figure 4), as derived from the analysis of NOESY spectra in the different mixed

micelle solution, were transformed in interprotonic distances for the calculation of C8 structural model using CYANA software (Figure 5).[22]

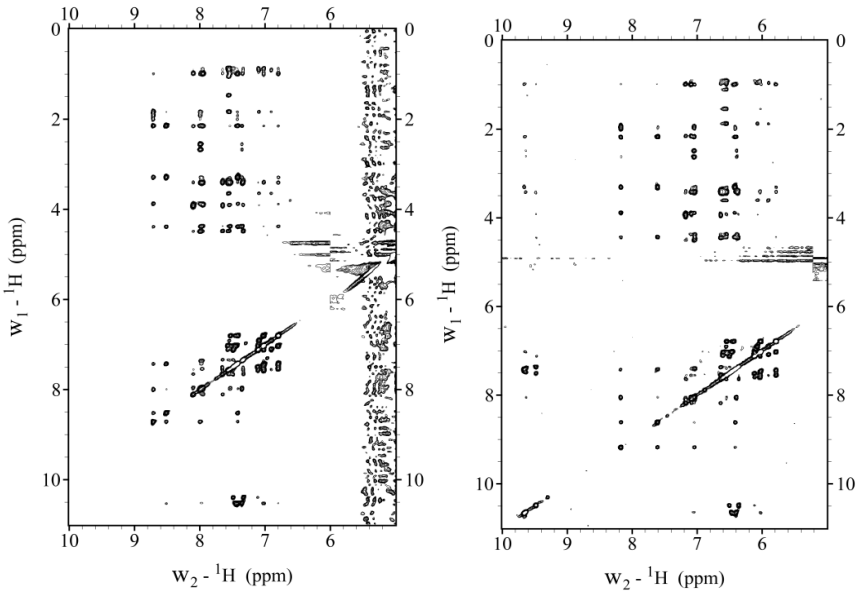

Figure 3. Low field region of NOESY spectra of C8 in DPC/SDS 10:90 M/M (A) and DPC/SDS 90:10 M/M (B) micelle solution. Spectra were recorded at 600MHz and 300K.

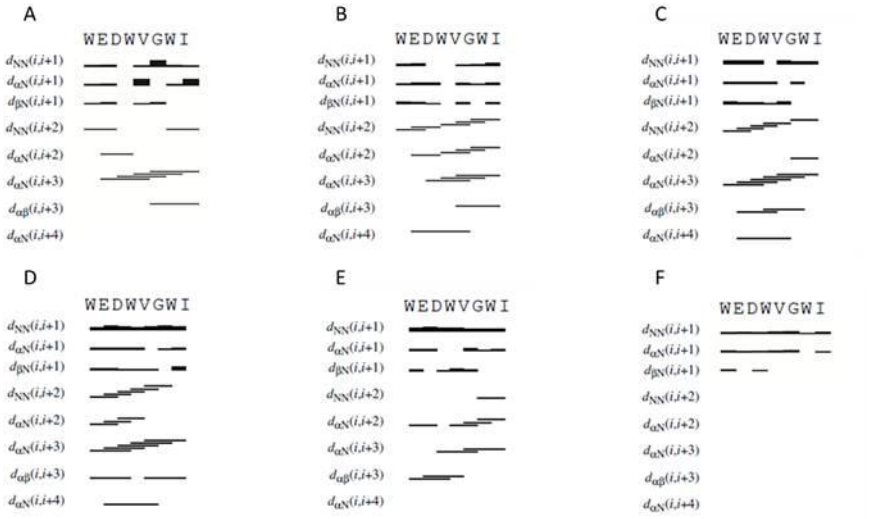

Figure 4. Sequential and medium range connectivities collected in NOESY spectra of C8 in DPC/SDS 100:0 (A), 90:10 (B), 60:40 (C), 40:60 (D), 10:90 (E) and 0:100 (F) M/M.

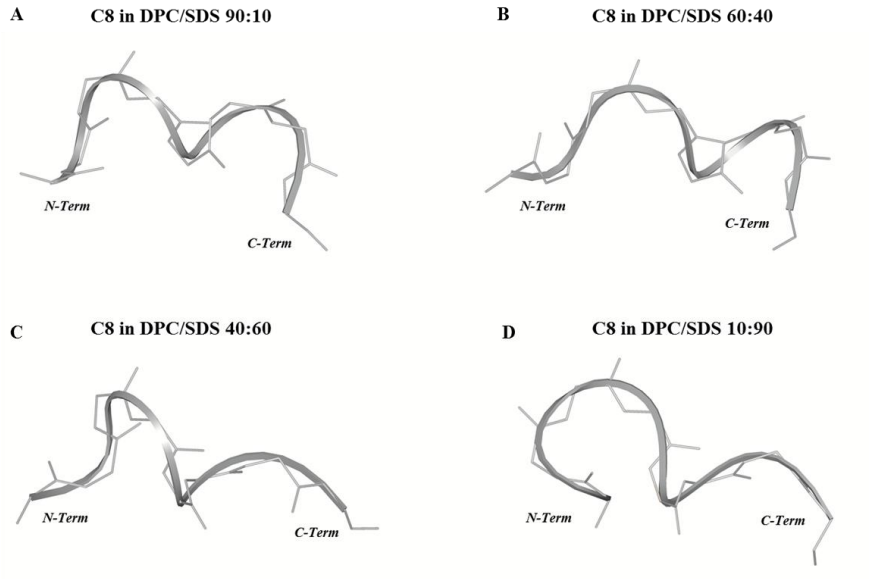

Figure 5. 3D model of C8 in DPC/SDS 90:10 (B), 60:40 (C), 40:60 (D), 10:90 (E) M/M using CYANA software.

The single NMR structures, analysed with PROMOTIF algorithm,[23] reveal the prevalence of type I β-turn on the residues Trp^{773}-Trp^{776} for C8 peptide in DPC/SDS at molar ratio 100:0, 90:10, 60:40 and 40:60; conversely in DPC/SDS at molar ratio 10:90 and 0:100, C8 is prevalently in random coil conformations with a minor proportion of γ-turn conformations encompassing Trp^{770}-Asp^{772} residues. In particular, for all DPC/SDS proportions 50 conformations of the C8 peptide have been calculated, the results show: i) in DPC/SDS 100:0 and 90:10 M/M all the structures (50/50) are stabilized by an H-bond between carbonyl of Trp^{773} and HN of Trp^{776} and between carbonyl of Trp^{773} and HN of Ile^{777}; ii) in DPC/SDS 60:40, 48/50 calculated structures show the same H-bonds as for the previous proportions; iii) in DPC/SDS 40:60 M/M, 15/50 calculated structures show H-bond between carbonyl of Trp^{773} and HN of Trp^{776}; iv) in DPC/SDS 10:90 M/M, 38/50 calculated structures show H-bond between carbonyl of Trp^{770} and HN of Asp^{772}, between carbonyl of Trp^{770} and HN of Trp^{773} and between carbonyl of Trp^{770} and HN of Val^{774}.

Taken together CD and NMR conformational data[11] in mixed DPC/SDS micelles confirm that the content of C8 regular secondary structure increases by increasing the proportion of DPC zwitterionic detergent. To define the role of the single Trp residues in the binding of C8 with lipid surface we monitored the chemical shift values variation of backbone protons in each system. Accordingly we observed that ^{1}H NH and CHα chemical shifts of Trp^{770} and Trp^{773} residues are those more sensitive to the composition of the micelle. Analysis of side chain orientation in C8 NMR structures confirm that Trp^{770} and Trp^{773} indole rings define a flat hydrophobic surface (Figure 6) prone to interact with hydrophobic micelle surface.

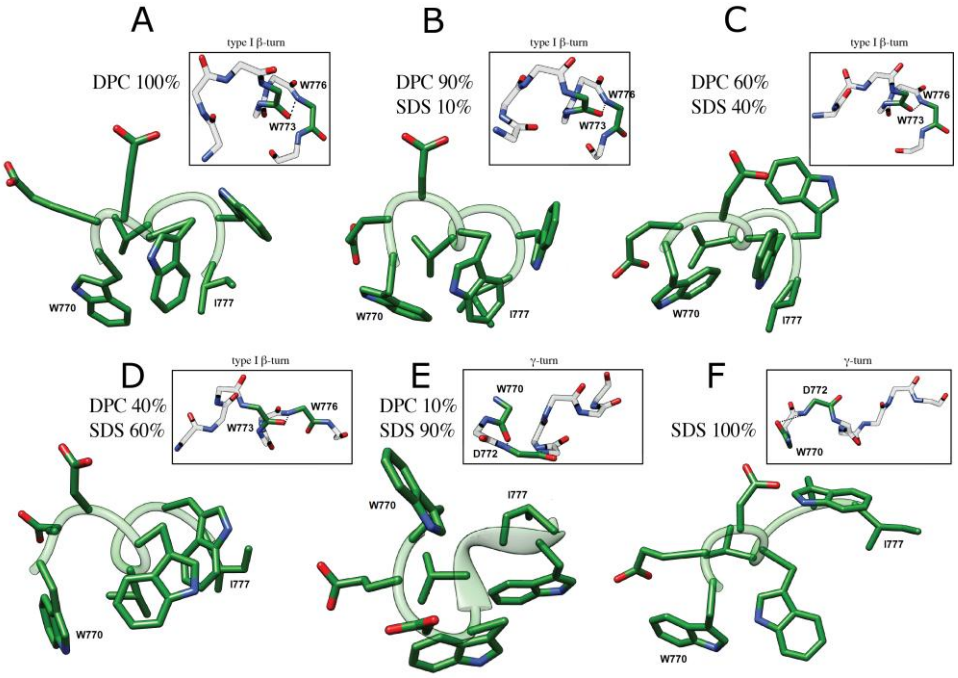

Figure 6. Low energy NMR models calculated for C8 in DPC/SDS 100:0 (A), 90:10 (B), 60:40 (C), 40:60 (D), 10:90 (E) and 0:100 (F) M/M. Calculation was carried out using standard CYANA protocol of simulated annealing in torsion angle space (10000 steps) applying interprotonic distances as restraints collected from NOE data.

2.1.2 Positioning of C8 on lipid surface: study with paramagnetic probes

To study the positioning of C8 with respect to the surface of micelles, we recorded NMR experiments in the presence of 5-doxyl-stearic acid (5-DSA) paramagnetic probes. These, owing to the presence of unpaired electrons, induce broadening of NMR signals and decrease in resonance intensities of residues close to the surface 5-DSA of the micelles.[13, 24, 25] Specifically we recorded TOCSY spectra of C8 in presence and absence of the spin labels, keeping all other conditions the same. Graphs reporting the variation in the NH intensities measured for C8 in 100:0 and 90:10 M/M mixed DPC/SDS micelle solutions with

or without 5-DSA (Figure 7) evidence the decrease of signals relative to the backbone protons of Trp^{770}, Trp^{773} and Gly^{775}. These data indicate that C8 interacts with the outer leaflet of micelles with a major role of Trp^{770} and Trp^{773} (Figure 7).

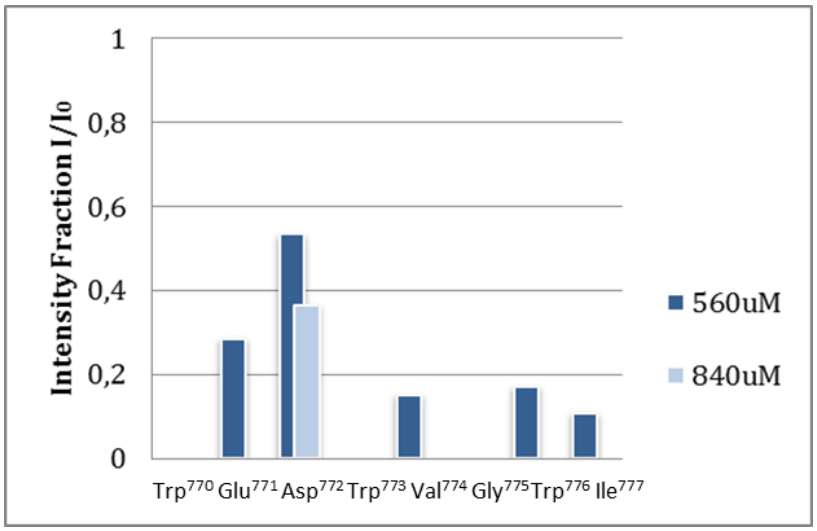

Figure 7. ^{1}H backbone NH intensities of C8 in DPC/SDS micelles recorded in the absence and the presence of 5-DSA. Legends in the frames are relative to spin label concentrations.

Moving toward more biomimetic lipid membrane systems, we investigated the interaction of C8 with the zwitterionic 1,2-Dioleoyl-sn-glycero-3-phosphocholine (DOPC), the negatively charged 1,2-Dioleoyl-sn-glycero-3-phosphoglycerol (DOPG) and the mixed DOPC/DOPG bilayers through Electron Spin Resonance (ESR) experiments. In particular, we detected changes in ESR spectra of spin-labelled lipids included in the membrane, specifically four phosphatidylcholine spin-labelled at different positions in the sn-2 chain, n-PCSL (n = 5, 7, 10, 14).[26-29] The comparison between the results obtained for the different spin-labelled

lipids allows the dynamics and the ordering of lipid acyl chains to be monitored in detail in the entire bilayer profile. Firstly, we analysed the effect of C8 on the 5-PCSL spectra in pure DOPC bilayers (Figure 8A). Both in absence and in presence of the peptide, spectra show an anisotropic line shape, typical of labels inserted in layered supramolecular structures, detectable from the evident splitting of the low- and high-field signals. In presence of the peptide, the anisotropic features become more evident, as highlighted by the evident shifts of the high-field maximum and low-field minimum. To quantitatively detect this effect, we measured the separation in Gauss between these points, called $2A_{max}$, which is an index of restriction of the local mobility of the acyl chains. The $2A_{max}$ value of 5-PCSL in DOPC bilayers increases by 1.5 G in presence of C8, revealing a stiffening of the bilayer outer region due to the peptide adsorption at the bilayer interface. Similar effects were observed for the same peptide interacting with bilayers formed by phosphocholine lipids with different acyl chains.[30] The perturbation, due to the peptide decreases in more disordered and fluid membranes, still remains, however, clearly detectable.

Secondly, the effects of the peptide on the 14-PCSL spectrum in pure DOPC were considered (Figure 8B). In absence of C8, an almost isotropic three-line shape is observed, due to the large motion freedom of the acyl chain termini in fluid lipid bilayers. In the peptide presence, the spectrum shows weak but significant changes: a shoulder can be observed at low field, while the high-field minimum is broadened. Both evidences point to perturbation of the bilayer inner core due to the C8-bilayer interaction. We further investigated the C8 effects by analysing also the spectra of 7-PCSL and 10-PCSL. The $2A_{max}$ variations along the entire lipid tail profile of DOPC are shown in figure 8C. $2A_{max}$ increases by almost the same extent at all spin-label position, indicating that the entire

membrane is significantly perturbed, in the direction of a lower bilayer fluidity and lipid dynamics.

Thirdly we investigated, using the same approach, the C8 interaction with lipid bilayers formed by DOPG and DOPC/DOPG at molar ratio 90:10, 60:40, 40:60 and 10:90. In the case of the pure anionic bilayer, no effect of the peptide was observed, the spin-labels spectra remaining unperturbed (Figure 8A and Figure 8B for the 5- and 14-PCSL spectra, respectively). This reflects in almost unchanged $2A_{max}$ values. Figure 8C shows the $2A_{max}$ value of 5-PCSL, in absence and in presence of C8, as a function of the DOPG percentage in DOPC/DOPG mixed bilayers. These experimental evidences show a gradual decrease of the observed lipid perturbation due to the interaction with C8 as the concentration of the anionic lipid increases. C8 is able to interact with bilayers containing maximum 60% DOPG, while in membrane with higher DOPG content the interaction is lost (Figure 8D).

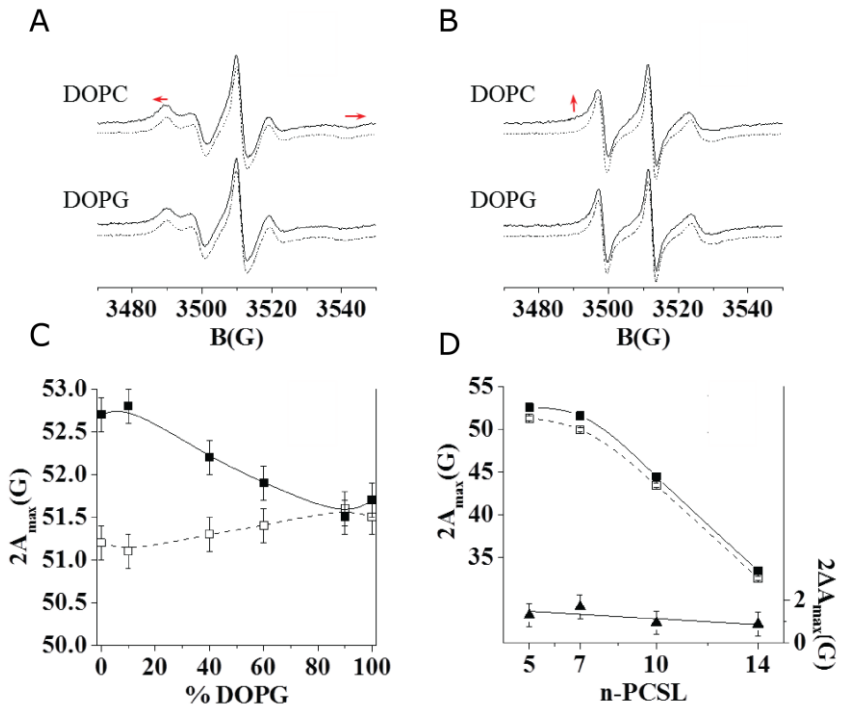

Figure 8. ESR spectra of 5-PCSL (panel A) and 14-PCSL (panel B) in lipid bilayers of DOPC and DOPG in absence (dashed lines) and presence (continuous lines) of the C8 peptide. In panel A the red arrows highlight the shift of the low-field maximum and high-field minimum. In panel B, the red arrow highlights the evidence of a second component in the spectrum registered in the presence of C8. n-PCSL dependency on spin-label position, n, of the outer hyperfine splitting, $2A_{max}$ (panel C, left-hand ordinate), in DOPC membranes in absence (dashed lines) and in presence of the C8 peptide (continuous lines); dependency on n of the $2A_{max}$ variation (panel D, right-hand ordinate). 5-PCSL dependency on the DOPG percentage in the lipid bilayer composition of the outer hyperfine splitting, $2A_{max}$ (panel D), in absence (dashed lines) and in presence of the C8 peptide (continuous lines).

2.1.3 Confocal microscopy

Confocal microscopy has been largely applied to investigate the biophysical properties of the membranes and the way in which these properties are exploited

by specific biological molecules to construct and direct biological functions at membrane level. According to an integrative approach of structural biology, to investigate at higher scale, the biophysical properties observed for C8 in different membrane models using CD, NMR and ESR spectroscopies, we carried out confocal microscopy imaging on nitrobenzodiazole (NBD)-labelled C8.[31] Six different multilamellar vesicles (MLVs), varying in DOPC/DOPG concentration ratio from 100:0 to 0:100 as done in the previous experiments, were imaged in absence and presence of the C8 peptide. Figure 9 shows that MLVs assume a spherical architecture in absence of peptide with diameter ranging within 5-20 µm.

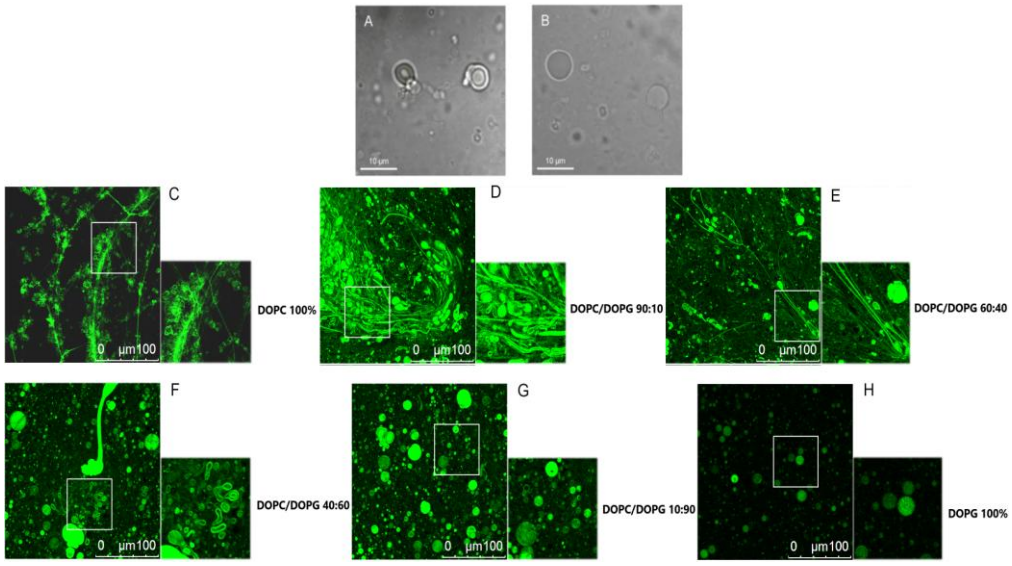

Figure 9. A-B Confocal microscopy imaging of MLVs in absence of NBD labelled-C8 peptide. In A and B MLVs are composed of DOPC/DOPG 90:10 and 0:100 M/M respectively. C-H: confocal microscopy imaging of MLVs in presence of (NBD)-labelled-C8 peptide. MLVs vary in DOPC/DOPG composition as reported in the labels.

Addition of C8 (NBD[1])-Trp induces fluorescence of the lipid membranes, indicating the localization of the peptide on the membrane surface (Figure 9 C-H). Comparison of confocal microscopy imaging pictures of vesicles composed by different DOPC/DOPG molar ratio (100:0, 90:10, 60:40, 40:60, 10:90 and 0:100) indicates that in the case of the pure DOPG, C8 peptide has minimal impact on the size and the shape of the vesicles that range in diameter within 5-20 μm. In vesicles formed by DOPC/DOPG mixed bilayers, a gradual modification of size and shape of vesicles is evident, as the concentration of the zwitterionic lipid increases. MLVs containing DOPC/DOPG 10:90 and 40:60 M/M are generally modified in their size. In these conditions many vesicles have diameter ranging from 20 to 40 μm, indicating that in these proportions of zwitterionic/negatively charged phospholipids, in presence of C8 peptide, membrane fusion occurs. Conversely, in vesicles characterized by increased proportion of zwitterionic DOPC (DOPC/DOPG 60:40, 90:10, 100:0 M/M), in addition to the vesicle fusion, C8 induces modification of membrane shape with the formation of membrane "nipples" (DOPC/DOPG 60:40 M/M), membrane tubes and complex tubular networks[32] (DOPC/DOPG 90:10 and DOPC/DOPG 100:0 M/M). In MLVs composed of DOPC/DOPG 90:10 M/M, which is representative of that found in mammalian cell membranes,[13, 33] these extended straight-chain tubular structures (Figure 9 C, D, E) are long dozens 100μm and capped at both ends with large liposomal structures. It is interesting to note that the phospholipid tubes formed in MLVs made of DOPC/DOPG 90:10 M/M have a diameter of 15±10 nm, that falls in the range of those estimated for tubular transport carriers operating, for example, between the Golgi and the plasma membrane in vivo.[34, 35]

2.2 Interaction study with membranes by molecular dynamics

2.2.1 Funnel-Molecular Dynamics (FMD)

Confocal microscopy provides a macroscopic description (i.e. in the order of μm) of the molecular interaction between C8 and membrane models. In order to provide insights into the peptide/membrane binding interaction at lower scale, in collaboration with the group of Professor Limongelli of USI in Lugano, we performed atomistic molecular dynamics simulations using membranes composed of diverse ratios of zwitteronic/negatively charged lipids, reproducing the same environment used in the C8-labelled imaging and ESR spectroscopy experiments. The investigation of the binding mechanism of C8 to the lipid bilayer was performed through funnel-molecular dynamics (FMD) calculations in explicit solvent, which is a novel approach already used with success in molecular binding studies.[27] Using such technique, one can indeed take into account properties of the systems like water contribution and protein/lipid conformational flexibility, that might play a key role in complex molecular binding events. However, processes such as peptide/membrane binding typically occur in long timescale (from μs to s), which limits the application of standard simulative protocols such as classic molecular dynamics. With the aim at enhancing the sampling of the binding process between C8 and membrane, here we have used FMD, an approach based on the use of a funnel-restrained potential that considerably reduces the conformational space to explore in the unbound state. Specifically, the funnel potential is applied to the system to include in the cone section the binding region of the target molecule, while the cylinder section points towards the solvent. In such a way, during the simulation, the ligand explores all the possible binding modes to the target structure while the exploration of the unbound region is reduced to the cylinder section (Figure 10A).

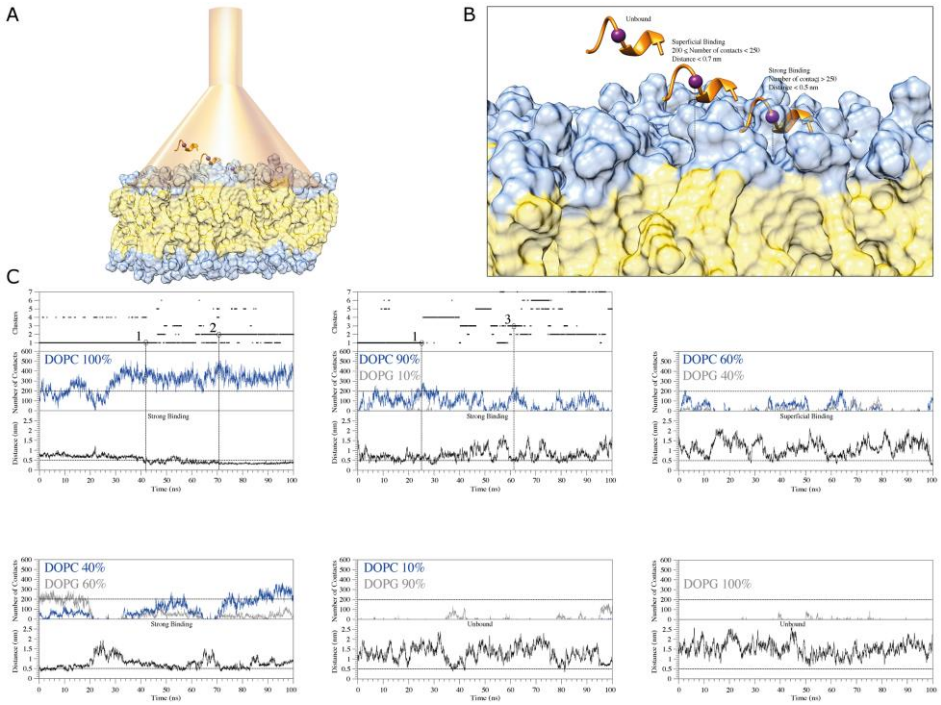

Figure 10. (A) Schematic representation of the FMD setting. The C8 peptide is represented in orange ribbon while the purple sphere represents the Cα atom of Val^{774}. The membrane is represented as molecular surface where the polar heads and the aliphatic chains of the phospholipids are coloured in light blue and in light yellow respectively. (B) Schematic representation of the binding states of the C8 peptide with the membrane. The peptide and the membrane are represented as in A. The distance between Cα atom of the Val^{774} and the polar heads of the phospholipids is reported as a dashed line. (C) Cluster analyses, number of contacts and distance between Cα atom of Val^{774} and the polar heads of phospholipids are reported as function of the simulation time for each of the six systems with the following zwitterionic/negatively charged phospholipids composition: pure DOPC, DOPC/DOPG 90:10, 60:40, 40:60, 10:90 M/M and pure DOPG. The vertical and horizontal dashed lines represent the cut offs for the characterization of the three C8 binding states. The intersection between the two dashed lines defines the representative structure of the cluster extracted to characterize the binding conformation and the binding mode of the C8 peptide.

This approach allows observing within a reasonable computational time a high number of binding and unbinding events between the ligand and the target molecule.[46]

FMD simulations were performed to describe the binding mechanism of the C8 peptide to the membrane models represented by DOPC, DOPC/DOPG 90:10, 60:40, 40:60 and 10:90 molar ratio, and pure DOPG. For each of the six systems, 100 ns of FMD calculations were performed using the NMR structure of C8 resolved in DPC/SDS micelle solutions as starting state.

Our data show the preference of peptide C8 to interact with membranes composed by higher concentration of DOPC rather than DOPG. Our results reveal that, in all the cases, C8 mostly interacts with the zwitterionic lipid polar heads of the DOPC phospholipids rather than with the negatively charged heads of DOPG (blue lines vs. grey lines in Figure 10C, respectively). In line with this observation, in systems with higher concentration of DOPG (i.e., 10:90 DOPC/DOPG M/M and pure DOPG) C8 remains in the unbound state for most of the simulation time and engages only superficial contacts with the membrane (grey lines in Figure 10C for DOPC/DOPG 10:90 M/M and pure DOPG). This behaviour is due to the electrostatic repulsion effect between the negatively charged residues of C8 (Glu^{771} and Asp^{772}) and the negatively charged polar heads of DOPG (Figure 10B).

As can be seen in Figure 11, the peptide binding conformations obtained from the simulations in pure DOPC membranes are remarkably similar to the NMR structure obtained in pure DPC micelles. We assessed this similarity computing the RMSD of Cα atoms in the binding conformation of cluster 1 and cluster 2 relative to the NMR structure. The value is 1.2 Å for the binding conformation A representative of cluster 1, while it is 2.2 Å for the binding conformation B

representative of cluster 2 (Figure 11A). In the latter case, RMSD becomes smaller (0.7 < Å) if considering the first 6 N-terminal residues, which form the type I β-turn structural motif and are involved in interaction with the membrane phospholipids according to our NMR and *in silico* data. Furthermore, for these residues (the first 6 N-terminal residues) we computed a low RMSD value of 0.82 Å of Cα atoms between the binding conformations A and B, leading to the conclusion that one single binding mode of C8 can be considered in pure DOPC membrane. The higher population of cluster 1 prompted us to consider hereafter A as the C8 binding mode in pure DOPC.

A similar approach was used to compare the peptide binding conformations identified by FMD in DOPC/DOPG 90:10 with that found by NMR in the equivalent phospholipid environment. In this case, RMSD calculated for Cα atoms between the binding conformation C representative of cluster 1 and the NMR structure is 2.4 Å. Similarly to what found for cluster 2 in DOPC, this value becomes smaller (0.6 Å) when only the first 6 N-terminal residues of C8 are considered in RMSD calculation (C in Figure 11A). At variance with pose C, the binding conformation D representative of cluster 3 is rather different from the NMR structure with RMSD value of 3.8 Å (D in Figure 11A). The dissimilarity of this pose with the NMR structure, the lack of hallmark for type I β-turn and of other ordered structural motif, together with the minor population of cluster 3 prompted us to discard this pose and hereafter consider C as the C8 binding mode in 90:10 DOPC/DOPG. A detailed structural description of the C8 binding mode in pure DOPC and 90:10 DOPC/DOPG were shown in Figure 11 B and C, respectively.

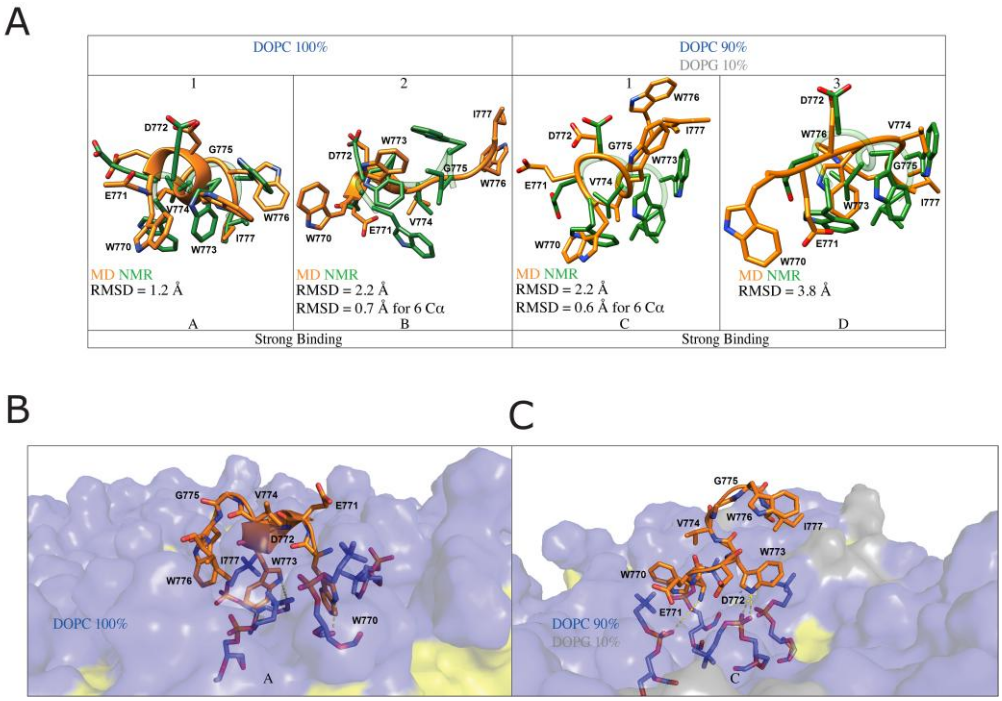

Figure 11. (A) Superposition between the C8 binding conformations derived from pure DOPC and DOPC/DOPG 90:10 M/M simulations and the NMR-derived ones. The peptides structures are depicted as cartoon. FMD- and NMR-derived C8 conformations are coloured in orange and green respectively. RMSDs of Cα atoms of each superposition are also reported. (B) The selected binding modes for the C8 peptide in pure DOPC are reported with the membrane. The phospholipids are represented as transparent surface. The aliphatic chains are coloured in yellow whereas the polar heads of DOPC and DOPG are coloured in light blue. The DOPC polar heads interacting with C8 are also reported in blue stick. H-bonds are highlighted with dashed yellow lines. (C) As in B but the represented C8 peptide binding mode was extracted from the DOPC/DOPG 90:10 M/M and the polar heads of DOPG are coloured in light grey.

2.2.2 In silico model vs. experimental data

Pure DOPC and DOPC/DOPG 90:10 M/M are the environment in which the peptide engages the strongest interactions with the bilayer (Figure 10C) inducing

the major rearrangement of the membrane architecture as observed at confocal microscopy (Figure 9). Although the size of simulation models and the simulated timescale do not allow observing macroscopic effects such as membrane curvature, it is possible to have with atomistic resolution structural insights into the molecular interaction of C8 with the pure DOPC and DOPC/DOPG 90:10 M/M membrane.

To this end, the binding conformations assumed by the peptide during the FMD simulations were clustered in families according to RMSD of C8 backbone atoms (Figure 10C).

The peptide binding conformations representative of the most populated clusters in pure DOPC and DOPC/DOPG 90:10 M/M, were superimposed with the C8 NMR structures obtained in the equivalent phospholipid environment (i.e., pure DOPC with pure DPC; DOPC/DOPG 90:10 M/M with DPC/SDS 90:10 M/M). As can be seen in Figure 11A, the peptide binding conformations obtained from the simulations in pure DOPC membranes are remarkably similar to the NMR structure obtained in pure DPC micelles.

To compare the peptide binding conformations identified by FMD in DOPC/DOPG 90:10 M/M with that found by NMR in DPC/SDS 90:10 M/M, the same approach was used. Similarly to what found in pure DOPC, also in DOPC/DOPG 90:10 M/M the interaction of C8 with the membrane is mediated by Trp residues (Figure 11C). In particular, Trp^{770} and Trp^{773} point to the membrane forming three H-bonds and three cation-π interactions with the DOPC zwitterionic polar heads. At variance with the previous binding mode, here Trp^{777} is solvent exposed and does not interact with the phospholipid atoms (Figure 11C). Similarly to what seen in the C8 binding mode in pure DOPC, the negatively

charged residues Glu[771] and Asp[772] can form electrostatic interactions with the phosphatidylcoline groups of DOPC.

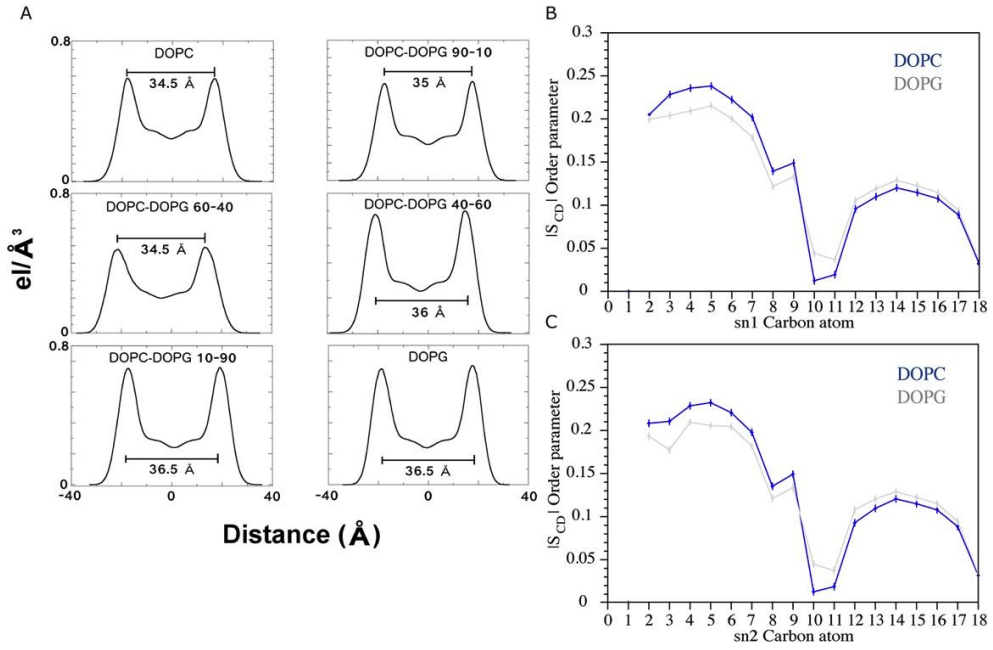

Figure 12. (A) Electron Density Profile (EDP) of the bilayers with different amount of DOPC and DOPG lipids. For each system the thickness was calculated (black bars) as distance between the two peaks. The value in Å below the bar indicates the final thickness. It can be appreciated how the reduction in thickness correlates with the strength of the interaction of C8 with the surface bilayer (Figure 11C). (B and C) Plots of the SCD parameter computed for the sn1 and sn2 chains of the DOPC and DOPG phospholipids during the binding simulations. The blue and grey lines represent DOPC and DOPG respectively.

The involvement of C8 Trp residues in the membrane binding is in agreement with the NMR data showing an exposition of Trp residues to the apolar environment formed by phospholipids. However, elucidating the microscopic interactions between the peptide and the membrane phospholipids does not allow

deciphering macroscopic behaviour of the membrane such as the formation of tubules observed through confocal microscopy. Clues to this end might come from the analysis of physical properties of the membrane and how they change upon the binding of C8. The thickness of the bilayer was analysed in all the six systems in order to evaluate its variation with growing percentages of zwitterionic phospholipids (i.e. DOPC) in the membrane bilayer. Passing from pure DOPG (36.5 Å) to pure DOPC (34.5 Å), the membrane becomes ~2 Å thinner (Figure 12A), thus the higher the concentrations of zwitterionic phospholipids, the stronger the C8/membrane interaction and the thinner the membrane is. This trend seems correlated to the propensity of the membrane to form tubules as observed by confocal microscopy. In fact, in presence of C8, higher concentrations of DOPC in the bilayer favour the aggregation of phospholipids to form membrane tubules.

Furthermore, the order parameter of the phospholipids S_{CD} was analysed. This estimates the organization of the lipids forming the membrane. In particular, the higher the S_{CD} value, the greater is the order degree of the lipids. In order to investigate the variation of the lipids organization related to the peptide binding, we compared the values of the parameter S_{CD} computed in pure DOPC and pure DOPG. These represent the two opposite cases, the former (DOPC) in which the peptide is bound to the membrane most of the simulation time, and the latter (DOPG) in which no binding event is observed (Figure 12B-C). The calculated S_{CD} values are in agreement with the experimental and computational data reported in literature[36, 37] and show that the C8 binding changes the organization of both the lipid carbon chains sn1 and sn2 from the polar head to the fifteenth carbon atom. These data demonstrate that the C8 binding induces conformational rearrangements of the lipids that might lead to macroscopic structural remodelling

of the bilayer as observed by confocal microscopy (Figure 9). However, further simulations on larger systems with prolonged timescale are necessary to provide more insightful data in this sense.

Discussion

In order to provide a full characterization of the molecular interaction of C8 with membrane, we investigated the binding mechanism of C8 with six different membrane models characterized by diverse superficial charge. Analyses of the C8 secondary structure using CD and NMR spectroscopy indicates that in membranes mostly formed by zwitterionic phospholipids C8 assumes a regular secondary structure. In particular in mixed DPC/SDS 90:10 M/M, corresponding to those more typical of biological membranes,[12] C8 is in type I β-turn conformation similar to that of pure zwitterionic micelles (DPC)[11]. The presence of small quantities of negatively charged phospholipids, does not affect the structural stability of the C8 peptide, and loss of ordered conformations occurs only when the zwitterionic/negatively charged phospholipid ratio is below 60:40.

In order to provide deeper insights into the molecular mechanism governing the interaction of C8 with membrane, we have carried out spin label NMR and ESR spectroscopy experiments. Our data indicate that in pure zwitterionic and mixed 90:10 M/M bilayers C8 strongly interacts with lipid interface through the indole rings of Trp^{770} and Trp^{773}. Furthermore, the ESR spectra show that in systems characterized by the prevalence of zwitterionic phospholipids (DOPC) the entire membrane is perturbed, with higher lipid ordering and lower dynamics, while this effect is much weaker for the pure negatively charged bilayers (DOPG). The strong interaction of C8 with zwitterionic membranes is further confirmed by confocal microscopy, which provides evidences of membrane tubulation in

presence of C8. This effect is not observed in MLVs composed of negatively charged phospholipids (DOPG), where the circular shape of the vesicles remains unmodified (Figure 9). The formation of membrane tubules induced by C8 is an unprecedented discovery for antiviral membrane binding peptides that raises new important questions to be addressed. Examples are: i) is membrane tubulation functional for the antiviral activity of the peptide? ii) Can C8 play a destabilizing effect also on the virus envelope architecture modulating its virulence? iii) Does membrane tubulation occur in the case of antiviral peptides of virus human variant HIV? iv) Can we exploit the ability of peptides to induce membrane tubulation in drug design to develop new antiviral agents? These are only some of the issues raised by our study that might open in the near future research opportunities unexplored so far.

Our experimental binding model is in agreement with the results coming from theoretical calculations. In particular, atomistic MD simulations carried out on six different systems composed by membranes with diverse molecular ratios of DOPC and DOPG, show higher binding affinity of C8 for bilayers enriched in zwitterionic phospholipids, DOPC (Figure 10C). Our molecular simulations show that C8 interacts with the membrane surface through the Trp residues, which establish cation-π and H-bond interactions with the DOPC zwitterionic polar head. In addition, salt bridge interactions established between the negatively charged amino acids of C8 (i.e., Glu^{771} and Asp^{772}) and the phospholipid zwitterionic polar heads contribute to stabilize the interaction between the membrane and the peptide. We have also provided a direct comparison of the peptide structure obtained by NMR and simulations in pure DOPC and DOPC/DOPG 90:10 M/M systems. The remarkable agreement between them further supports the proposed binding mode in which the Trp residues govern the

interaction with the bilayer establishing key intermolecular interactions with the phospholipid polar heads (Figure 11B and C). According to the ESR data, the membrane organization is affected by the C8 binding. In particular, a strong stiffening of the bilayer outer region is found, due to the C8 adsorption onto the bilayer surface. In our simulations, we have analysed physical properties of the membrane like thickness and lipids order degree, in dependence of the interaction with C8. In particular, we have found that the peptide binding induces a microscopic reorganization of the membrane depending on the bilayer charge composition (Figure 12B-C). This leads to an overall rearrangement of the membrane as demonstrated by the thinner thickness of bilayers enriched in DOPC if compared to those enriched in DOPG (Figure 12A). Based on these data and considering the observation of membrane tubules at confocal microscopy in pure zwitterionic and DOPC/DOPG 90:10 M/M, it is tempting to suggest the proposed C8 binding mode as the very first step of the C8/membrane interaction that induces membrane reorganization and remodelling, finally leading to macroscopic effects like curvature change and formation of membrane tubules as observed with confocal microscopy.

Our bottom-up approach is necessary if one aims at controlling in a rational way the lipid architecture in complex processes such as ligand membrane penetration and tubule formation. The latter is a membrane remodelling phase, most important in cell trafficking and cell communication processes that, in spite of their ubiquity, remains rather unexplored.[33] Our study will have foreseeable impact in the rational design of novel peptides with controlled affinity towards cell membrane. Having such control in peptide design is of paramount relevance to develop new antiviral peptides, as well as in pharmaceutical technology, where peptides can be used as “smart” molecules able to form vesicular structures and

lipid-based bio-nanotubes working as molecular storage and dispenser of chemicals and drugs into living cells.[38]

References

1. D'Ursi, A. M.; Giannecchini, S.; Di Fenza, A.; Esposito, C.; Armenante, M. R.; Carotenuto, A.; Bendinelli, M.; Rovero, P. Retroinverso analogue of the antiviral octapeptide C8 inhibits feline immunodeficiency virus in serum. *J Med Chem* **2003,** 46, 1807-10.

2. D'Ursi, A. M.; Giannecchini, S.; Esposito, C.; Alcaro, M. C.; Sichi, O.; Armenante, M. R.; Carotenuto, A.; Papini, A. M.; Bendinelli, M.; Rovero, P. Development of antiviral fusion inhibitors: short modified peptides derived from the transmembrane glycoprotein of feline immunodeficiency virus. *Chembiochem* **2006,** 7, 774-9.

3. Lee, T.; Laco, G. S.; Torbett, B. E.; Fox, H. S.; Lerner, D. L.; Elder, J. H.; Wong, C. H. Analysis of the S3 and S3 ' subsite specificities of feline immunodeficiency virus (FIV) protease: Development of a broad-based protease inhibitor efficacious against FIV, SIV and HIV in vitro and ex vivo. *Proceedings of the National Academy of Sciences of the United States of America* **1998,** 95, 939-944.

4. Esposito, C.; D'Errico, G.; Armenante, M. R.; Giannecchini, S.; Bendinelli, M.; Rovero, P.; D'Ursi, A. M. Physicochemical characterization of a peptide deriving from the glycoprotein gp36 of the feline immunodeficiency virus and its lipoylated analogue in micellar systems. *Biochim Biophys Acta* **2006,** 1758, 1653-61.

5. Giannecchini, S.; Bonci, F.; Pistello, M.; Matteucci, D.; Sichi, O.; Rovero, P.; Bendinelli, M. The membrane-proximal tryptophan-rich region in the transmembrane glycoprotein ectodomain of feline immunodeficiency virus is important for cell entry. *Virology* **2004,** 320, 156-166.

6. Barbato, G.; Bianchi, E.; Ingallinella, P.; Hurni, W. H.; Miller, M. D.; Ciliberto, G.; Cortese, R.; Bazzo, R.; Shiver, J. W.; Pessi, A. Structural analysis of the epitope of the anti-HIV antibody 2F5 sheds light into its mechanism of neutralization and HIV fusion. *J Mol Biol* **2003,** 330, 1101-15.

7. Giannecchini, S.; D'Ursi, A. M.; Esposito, C.; Scrima, M.; Zabogli, E.; Freer, G.; Rovero, P.; Bendinelli, M. Antibodies generated in cats by a lipopeptide reproducing the membrane-proximal external region of the feline immunodeficiency virus transmembrane enhance virus infectivity. *Clin Vaccine Immunol* **2007,** 14, 944-51.

8. Merlino, A.; Vitiello, G.; Grimaldi, M.; Sica, F.; Busi, E.; Basosi, R.; D'Ursi, A. M.; Fragneto, G.; Paduano, L.; D'Errico, G. Destabilization of lipid membranes by a peptide derived from glycoprotein gp36 of feline immunodeficiency virus: a combined molecular dynamics/experimental study. *J Phys Chem B* **2012,** 116, 401-12.

9. Giannecchini, S.; Di Fenza, A.; D'Ursi, A. M.; Matteucci, D.; Rovero, P.; Bendinelli, M. Antiviral activity and conformational features of an octapeptide derived from the membrane-proximal ectodomain of the feline immunodeficiency virus transmembrane glycoprotein. *J Virol* **2003,** 77, 3724-33.

10. Giannecchini, S.; Alcaro, M. C.; Isola, P.; Sichi, O.; Pistello, M.; Papini, A. M.; Rovero, P.; Bendinelli, M. Feline immunodeficiency virus plasma load reduction by a retroinverso octapeptide reproducing the Trp-rich motif of the transmembrane glycoprotein. *Antivir Ther* **2005,** 10, 671-80.

11. Scrima, M.; Di Marino, S.; Grimaldi, M.; Campana, F.; Vitiello, G.; Piotto, S. P.; D'Errico, G.; D'Ursi, A. M. Structural features of the C8 antiviral peptide in a membrane-mimicking environment. *Biochim Biophys Acta* **2014,** 1838, 1010-8.

12. Bohr, H. *Handbook of molecular biophysics*. Wiley-VCH: 2009.

13. Pandey, S.; Alcaro, M. C.; Scrima, M.; Peroni, E.; Paolini, I.; Di Marino, S.; Barbetti, F.; Carotenuto, A.; Novellino, E.; Papini, A. M.; D'Ursi, A. M.; Rovero, P. Designed

glucopeptides mimetics of myelin protein epitopes as synthetic probes for the detection of autoantibodies, biomarkers of multiple sclerosis. *J Med Chem* **2012,** 55, 10437-47.

14. Mannhold, R.; Kubinyi, H.; Folkers, G.; Zerbe, O. *BioNMR in drug research*. John Wiley & Sons: 2006; Vol. 16.

15. Whitmore, L.; Wallace, B. A. DICHROWEB, an online server for protein secondary structure analyses from circular dichroism spectroscopic data. *Nucleic Acids Res* **2004,** 32, W668-73.

16. Bax, A.; Davis, D. G. MLEV-17-based two-dimensional homonuclear magnetization transfer spectroscopy. *Journal of Magnetic Resonance (1969)* **1985,** 65, 355-360.

17. Jeener, J.; Meier, B.; Bachmann, P.; Ernst, R. Investigation of exchange processes by two-dimensional NMR spectroscopy. *The Journal of chemical physics* **1979,** 71, 4546-4553.

18. Piantini, U.; Sorensen, O.; Ernst, R. R. Multiple quantum filters for elucidating NMR coupling networks. *Journal of the American Chemical Society* **1982,** 104, 6800-6801.

19. Piotto, M.; Saudek, V.; Sklenář, V. Gradient-tailored excitation for single-quantum NMR spectroscopy of aqueous solutions. *Journal of biomolecular NMR* **1992,** 2, 661-665.

20. Goddard, T.; Kneller, D. SPARKY 3. *University of California, San Francisco* **2004,** 15.

21. Wuthrich, K. *NMR of proteins and nucleic acids*. Wiley: 1986.

22. Güntert, P. Automated NMR structure calculation with CYANA. *Protein NMR Techniques* **2004**, 353-378.

23. Hutchinson, E. G.; Thornton, J. M. PROMOTIF—a program to identify and analyze structural motifs in proteins. *Protein Science* **1996,** 5, 212-220.

24. Solomon, I. Relaxation processes in a system of two spins. *Physical Review* **1955,** 99, 559.

25. Esposito, C.; Scrima, M.; Carotenuto, A.; Tedeschi, A.; Rovero, P.; D'Errico, G.; Malfitano, A. M.; Bifulco, M.; D'Ursi, A. M. Structures and micelle locations of the nonlipidated and lipidated C-terminal membrane anchor of 2', 3'-cyclic nucleotide-3'-phosphodiesterase. *Biochemistry* **2008,** 47, 308-319.

26. Marsh, D.; Horvath, L. I. Structure, dynamics and composition of the lipid-protein interface. Perspectives from spin-labelling. *Biochim Biophys Acta* **1998,** 1376, 267-96.

27. Bruno, A.; Scrima, M.; Novellino, E.; D'Errico, G.; D'Ursi, A. M.; Limongelli, V. The glycan role in the glycopeptide immunogenicity revealed by atomistic simulations and spectroscopic experiments on the multiple sclerosis biomarker CSF114(Glc). *Sci Rep* **2015,** 5, 9200.

28. Vitiello, G.; Grimaldi, M.; Ramunno, A.; Ortona, O.; De Martino, G.; D'Ursi, A. M.; D'Errico, G. Interaction of a β-sheet breaker peptide with lipid membranes. *Journal of peptide science: an official publication of the European Peptide Society* **2010,** 16, 115-122.

29. Vitiello, G.; Grimaldi, M.; D'Ursi, A. M.; D'Errico, G. The iAβ5p β-breaker peptide regulates the Aβ (25–35) interaction with lipid bilayers through a cholesterol-mediated mechanism. *Biochemical and biophysical research communications* **2012,** 417, 88-92.

30. D'Errico, G.; Vitiello, G.; D'Ursi, A. M.; Marsh, D. Interaction of short modified peptides deriving from glycoprotein gp36 of feline immunodeficiency virus with phospholipid membranes. *Eur Biophys J* **2009,** 38, 873-82.

31. Dufau, I.; Mazarguil, H. Design of a fluorescent amino acid derivative usable in peptide synthesis. *Tetrahedron Letters* **2000,** 41, 6063-6066.

32. Roux, A.; Cappello, G.; Cartaud, J.; Prost, J.; Goud, B.; Bassereau, P. A minimal system allowing tubulation with molecular motors pulling on giant liposomes. *Proceedings of the National Academy of Sciences* **2002,** 99, 5394-5399.

33. Yue, T.; Zhang, X.; Huang, F. Molecular modeling of membrane tube pearling and the effect of nanoparticle adsorption. *Phys Chem Chem Phys* **2014,** 16, 10799-809.

34. Amodio, G.; Venditti, R.; De Matteis, M. A.; Moltedo, O.; Pignataro, P.; Remondelli, P. Endoplasmic reticulum stress reduces COPII vesicle formation and modifies Sec23a cycling at ERESs. *FEBS letters* **2013,** 587, 3261-3266.

35. Amodio, G.; Sasso, E.; D'Ambrosio, C.; Scaloni, A.; Moltedo, O.; Franceschelli, S.; Zambrano, N.; Remondelli, P. Identification of a microRNA (miR-663a) induced by ER stress and its target gene PLOD3 by a combined microRNome and proteome approach. *Cell biology and toxicology* **2016,** 32, 285-303.

36. Rosso, L.; Gould, I. R. Structure and dynamics of phospholipid bilayers using recently developed general all-atom force fields. *Journal of computational chemistry* **2008,** 29, 24-37.

37. Dickson, C. J.; Madej, B. D.; Skjevik, Å. A.; Betz, R. M.; Teigen, K.; Gould, I. R.; Walker, R. C. Lipid14: the amber lipid force field. *Journal of chemical theory and computation* **2014,** 10, 865-879.

38. Ariga, K.; Hill, J. P.; Lee, M. V.; Vinu, A.; Charvet, R.; Acharya, S. Challenges and breakthroughs in recent research on self-assembly. *Science and Technology of Advanced Materials* **2016**.

3 *C6a and C6b: interaction studies with membrane models*

3.1 C6a and C6b in DPC-SDS micelle

C8, the octapeptide belonging to gp36-MPER and eliciting antiviral activity was the object of extensive SAR studies.[1,2] In particular, studies aimed at the determination of the minimal active sequence confirmed the importance of Trp residues[3] and allowed identification of C6a, the fragment corresponding to Asp^{772}-Ile^{777} as characterized by twofold IC_{50} activity compared to C8 (Experiments performed to test inhibition of the replication of primary FIV isolated in lymphoid cells showed IC_{50} 0.06 for C8, and IC_{50} 0.15 for C6a).[2] On the contrary C6b, the fragment corresponding to Trp^{770}-Gly^{775}, was nearly inactive.[2] C6a and C6b are structurally similar: i) both are fragments of C8; they are characterized by the same amino acid composition, except for one residue; ii) both include two of the three Trp residues.

In the present part of my PhD thesis, I report the conformational analyses of C6a and C6b by CD and NMR spectroscopy in micelle solution composed of DPC/SDS 90:10 M/M. On a higher dimension scale, C6a and C6b were studied using confocal microscopy imaging on vesicles characterized by different phospholipid compositions.[4] These data allow identifying the conformational factors determining the different C6a and C6b membrane binding properties and hence the different antiviral activity profiles.

One major concern relative to anti-HIV fusion inhibitors is their peptide chemical structure and the high number of residues.[5] A valuable quality of C8 and its derivatives is the small size. The structural features of C6a and C6b derived from our analyses, matched to those of their parent peptide C8, lead to describe a pharmacophore model for anti-HIV fusion inhibitors; this includes the essential structural motifs to design new simplified molecules overcoming the limitations affecting the entry inhibitors currently used in clinical application.

3.2 C6a and C6b conformational analysis

We studied conformation of C6a and C6b in mixed DPC/SDS (90:10 M/M) micelles using CD spectroscopy.[6]

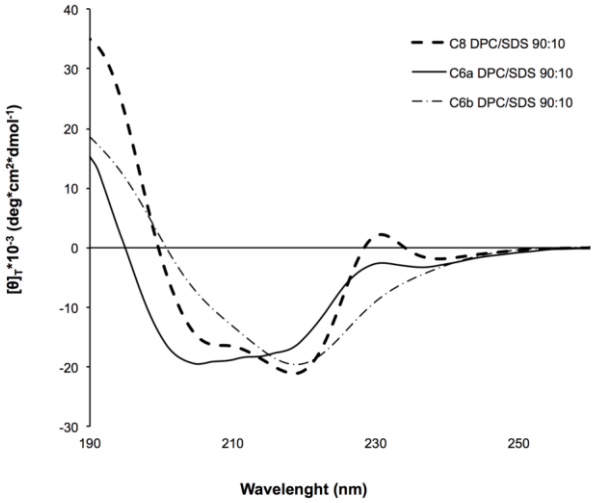

Figure 1. Processed far-UV CD spectra of C8, C6a and C6b peptides in DPC/SDS 90:10 M/M micelle. The CD spectra were acquired using a JASCO 810 spectropolarimeter at room temperature with a cell path length of 1 mm. The measurement range spans from 190 to 260 nm.

Figure 1 shows the far UV CD spectra of C6a and C6b recorded in DPC/SDS 90:10 M/M micelle solution. The shapes of CD spectra are consistent with the prevalence in C6a of regular turn-helix conformation, and non-canonical secondary structures in C6b. Quantitative evaluation of the CD spectra using CONTINN algorithm (DICHROWEB website)[7] confirm these indications.

NMR spectra of C6a and C6b in the same mixed DPC/SDS micelle solution (90:10 M/M) were acquired using a Bruker DRX-600 spectrometer. 2D COSY, TOCSY and NOESY data were recorded to allow for chemical shift assignment according to the conventional procedure of Wuthrich.[8] Proton chemical shifts are reported in Tables I–II. COSY, TOCSY and NOESY spectra were analysed using SPARKY software.[9]

Table I. ^{1}H chemical shift of C6a in DPC/SDS 90:10 M/M micelle solution.

Residue	HN	CαH	CβH	CγH	CδH	CεH	Others
Asp772	8.407	4.499	Qβ 2.723				
Trp773	8.085	4.280	Hβ2 3.305 Hβ3 3.131		Hδ1 7.005	Hε1 10.541 Hε3 7.380	Hη2 6.947 Hζ2 7.247 Hζ3 6.854
Val774	7.523	3.745	1.865	Hγ12 0.720 Hγ13 0.621			
Gly775	7.949	Qα 3.802					
Trp776	7.750	4.474	Hβ2 3.796 Hβ3 3.306		Hδ1 7.076	Hε1 10.362 Hε3 7.386	Hη2 6.897 Hζ2 7.254 Hζ3 6.854
Ile777	7.450	3.886	1.828	Qγ1 1.406 Qγ2 1.082	Qδ1 0.848		

Table II. ^{1}H chemical shift of C6b in DPC/SDS 90:10 M/M micelle solution.

Residue	HN	CαH	CβH	CγH	CδH	CεH	Others
Trp770	8.407	4.263	Qβ 3.193		Hδ1 6.763	Hε1 10.454 Hε3 7.397	Hζ2 7.360
Glu771	8.420	3.852	Hβ2 1.817 Hβ3 1.738	Hγ2 2.087 Hγ3 2.039			
Asp772	8.022	4.464	Qβ 2.765				
Trp773	7.928	4.416	Hβ2 3.373 Hβ3 3.273		Hδ1 6.972	Hε1 10.447 Hε3 7.534	Hζ2 7.255
Val774	7.735	3.859	2.126	Qγ1 0.944 Qγ2 0.905			
Gly775	7.784	Qα 3.801					

The sequential and medium-range connectivities observed in NOESY spectra (Figure 2) point to the presence of folded structures in both the peptides.

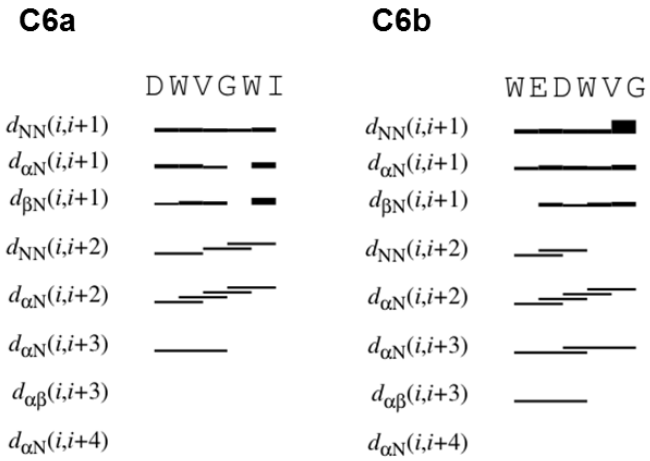

Figure 2. Sequential and medium range connectivities collected in NOESY spectra of C6a and C6b in DPC/SDS 90:10 M/M.

NOE data were transformed in interprotonic distances for the calculation of C6a and C6b NMR structures using CYANA software.[10] Figure 3 shows the NMR structure bundles of C6a and C6b. 20 structures out of the 50 calculated

were selected according to the lowest values of the target function.[10] The selected conformers were superimposed at level of the backbone heavy atoms showing 0.32 Å and 0.47 Å RMSD for C6a and C6b respectively.

Analysis of backbone dihedral angles using PROMOTIF[11] indicates the prevalence in C6a of regular β-turn structures encompassing the residues Trp^{773}-Trp^{776} and stabilized by H-bonds between carbonyl of Asp^{772} and HN of Gly^{775} and Trp^{776} (22 out of the 50 calculated structures) (Figure 3). Inspection of the side chains in C6a NMR structures evidences a parallel orientation of the Trp indole rings, to expose a large hydrophobic surface.

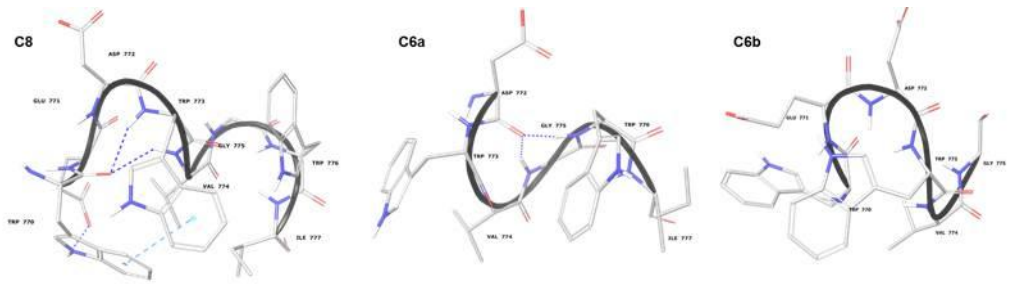

Figure 3. Low energy NMR models calculated for C8, C6a and C6b peptides in DPC/SDS 90:10 M/M micelle. Calculation was carried out using standard CYANA protocol of simulated annealing in torsion angle space.

Analysis of C6b NMR structure bundle indicates the prevalence of non-canonical secondary structures (Table III). The amino acid side chains form a globular amphipathic structure exposing, on one side, the negatively charged side chains of Glu^{771} and Asp^{772}, and on the other side the hydrophobic indole rings of Trp^{770} and Trp^{773}.

Table III. Backbone dihedral angles of C6a and C6b in DPC/SDS 90:10 M/M micelle solution.

C6a

Residue	Φ(phi)	Ψ(psi)
Asp772		
Trp773	-48	-27
Val774	-127	12.3
Gly775	-126	-25
Trp776	-51	-23
Ile777		

C6b

Residue	Φ(phi)	Ψ(psi)
Trp770		
Glu771	-78	55.9
Asp772	-174	-18
Trp773	-123	-63
Val774	-80	-20
Gly775		

3.3 C6a and C6b surface analysis

NMR analysis in DPC/SDS 90:10 M/M micelle solutions was the starting point to investigate the positioning of peptides with respect to the surface and interior of the micelle using 5-doxylstearic acid (5-DSA) and 16-doxylstearic acid (16-DSA) as paramagnetic probes. Both of these compounds contain a doxyl head group and a cyclic nitroxide with unpaired electrons that is bound to the aliphatic carbon chain at either position 5 or 16. NMR experiments were recorded in micelle solutions containing 5-DSA or 16-DSA.

Paramagnetic probes are able to induce a broadening of the NMR signal and a decrease in the resonance intensities. Generally, the peptide sites that are closest to NO moiety are affected by the unpaired electron, with an increase in nuclear relaxation rates and, thus, a decrease in proton signals.

If the peptide is close to the surface, a decrease in intensity is observed in 5-DSA spin-labeled micelles, while if the peptide penetrates the inner core of the micelle, a decrease in intensity is observed in 16-DSA spin-labeled micelle.[6] 1D and 2D TOCSY spectra of the C6a and C6b peptides were recorded in DPC/SDS 90:10 M/M micelle solutions in presence and absence of 5-DSA and 16-DSA

while keeping all other conditions constant. Comparison of 1D ^{1}H NMR proton spectra of the C6a and C6b peptides recorded in presence and absence of 5-DSA shows a selective perturbation of Trp CHα-NH and Trp-indole proton signals in presence of 5-DSA. (Figure 4). Comparison of TOCSY spectra of C6a and C6b recorded in DPC/SDS 90:10 molar ratio micelle solutions in presence of 5-DSA shows that Trp Hε1 signals are decreased in intensities due to the presence of the spin label. This effect is nearly 60% in C6a and 30% in C6b. Backbone NHs of Trp are 30% and 15% decreased in intensities for C6a and C6b respectively. This effect is consistent with the localization of the peptide on the micelle surface, as observed in the confocal microscopy imaging.

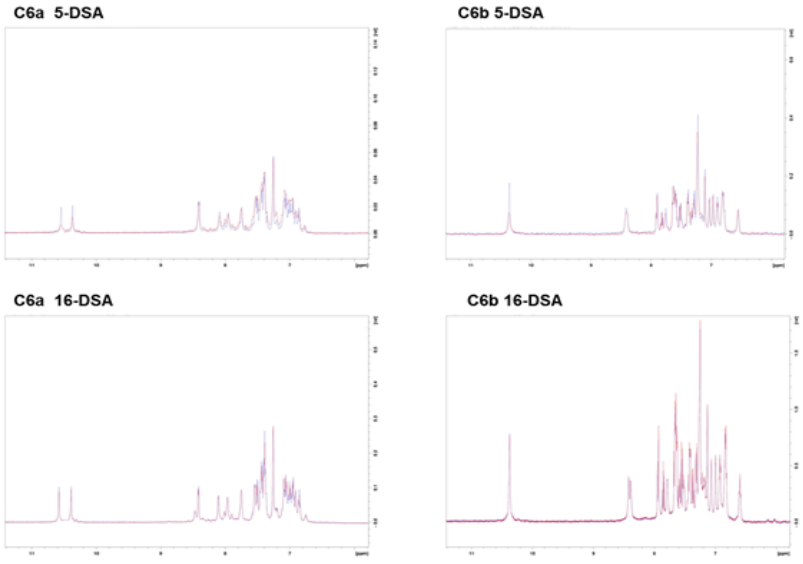

Figure 4. Low field region of 600 MHz 1D proton spectra of the C6a and C6b peptides recorded in DPC/SDS 90:10 M/M micelle solutions at 300 K in absence (blue) and in presence of 5-DSA and 16-DSA (red) at a concentration of one spin label *per* micelle.

According to the aminoacid sequences, we can infer that in C6a, the ^{774}Val-Gly^{775} residues act as a flexible linker between Trp^{773} and Trp^{776}, favouring a regular β-turn conformation. In C6b, ^{771}Glu-Asp^{772} residues form a more rigid linker between Trp^{770} and Trp^{773}, preventing the formation of regular secondary structures.

Analysis of the most representative C6a and C6b NMR structures evidences that C6a is characterized by an elongated molecular shape, with the indole rings of Trp^{773} and Trp^{776} in a nearly parallel orientation (the planes that run through the Trp^{773} and Trp^{776} draw an angle of 13.64°). These generate a hydrophobic molecular surface (Figure 5), calculated for 220.5 Å^2.

The negatively charged Asp^{772} side chain flanks the Trp^{773} indole ring directly in this molecular area. Contrarily to C6a, C6b has a globular shape, and the planes that run through the Trp^{770} and Trp^{773} indole rings draw an angle of 62°. The 220.5 Å^2 molecular surface generated by these residues is smaller as compared to C6a. The negatively charged side chains of Glu^{771} and Asp^{772} are on the opposite side with respect to the Trp indole rings (Figure 5).

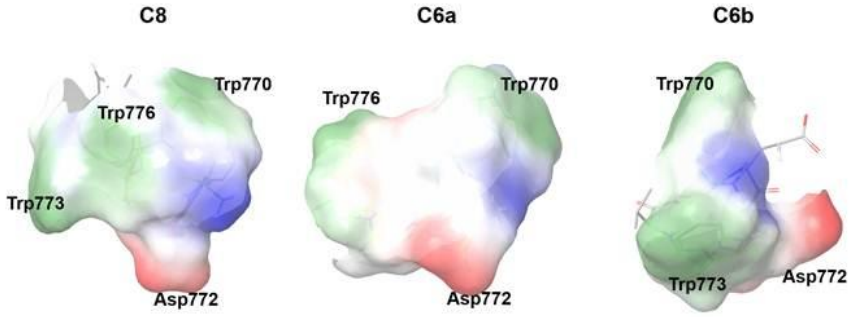

Figure 5: Molecular surface calculated as propensities of different portions of the molecules to interact according to the specific surface properties. Molecular surfaces of Trp residues are coloured in green-white: they account for the propensity of peptides to engage hydrophobic interactions. Molecular surfaces of Asp residues are coloured in blue: they account for the propensity of peptides to engage polar/electrostatic interactions.

Many peptide molecules have been studied as antiviral fusion inhibitors. However, those approved for antiviral therapy have high molecular weight, with complications deriving from the high economic cost and the difficulty of administration. Comparison of the most representative conformations of C8 and C6a (Figure 6) indicates that it is possible to draw a pharmacophore model including the indole rings of the two Trp residues (which in C8 belong to Trp^{770} and Trp^{776}, and in C6a belong to Trp^{773} and Trp^{776}) and the side chain of Asp^{772}. This model may be the starting point to design new small peptide-peptidomimetic molecules endowed with improved pharmacodynamic/ pharmacokinetic properties.

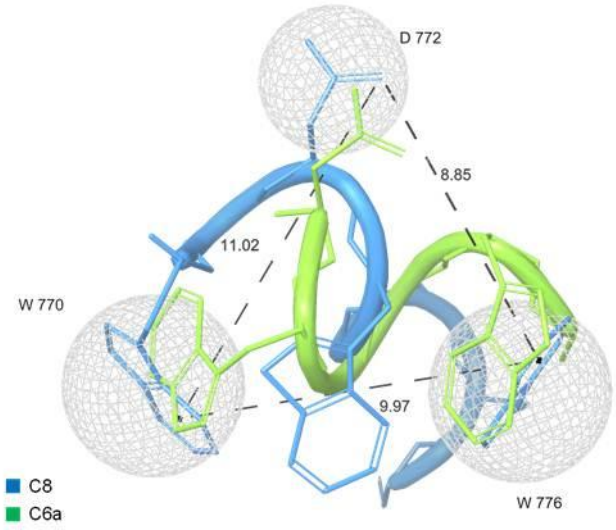

Figure 6. Pharmacophore model of anti-FIV fusion inhibitors. Overlapping of C8 (light blue) and C6a (green) NMR representative models. Molecular surfaces (grey) surround the carboxylic moiety of Asp^{772} side chain and indole rings of Trp^{770} and Trp^{776} in C8, and Trp^{773} and Trp^{776} in C6a.

Using atomistic molecular simulations,[12] we previously demonstrated that the binding of C8 with phospholipid bilayers is mediated by i) hydrophobic interactions involving the Trp indole rings and the hydrophobic chains of phospholipids ii) salt bridge interactions established between the negatively charged aminoacids (i.e., Glu^{771} and Asp^{772}) and the phospholipid zwitterionic polar heads. The pharmacophore shown in Figure 6 is consistent with this model of interaction for C6a and C8, but not for C6b; notably, the absence of the ^{770}Trp-Glu^{771} N-terminal residues may explain the two-fold lower activity of C6a as compared to the C8 for FIV-M2. Accordingly we can speculate that activity at vesicle surface and at cell membrane rely in the synergic molecular interactions,

involving Trp indole rings and negatively charged aminoacid: these induce destabilization of the bilayer, determining membrane tubes and membrane fusion.

An estimation of the molecular surface, calculated according to the aptitude of peptides to engage electrostatic/polar interactions with positively/negatively charged surfaces, or hydrophobic interactions with hydrophobic surfaces (Table IV)[13] indicates that C6a and C6b expose 286.2 $Å^2$ and 220.5 $Å^2$ of hydrophobic surface respectively. A similar calculation for the NMR structure of the parent peptide C8, indicates that the extension of the hydrophobic surface of C8 is 288.3 $Å^2$, very similar to that of C6a. Moreover, the molecular surfaces of C6a and C6b and of their parent peptide C8 show several spots of electrostatically charged surfaces. According to molecular dynamic calculations performed by us,[12] these charged sites engage electrostatic interactions with phospholipid polar heads. Hence hydrophobic and electrostatic interactions are synergistic to destabilize the phospholipid bilayer and modify membrane size and shape.

Table IV. Molecular surface values calculated as propensities to engage molecular interaction according to specific surface properties.

Peptide	Hydrophobic surface	Negatively charged surface	Positively charged surface
C8	288.3 $Å^2$	210.8 $Å^2$	137.9 $Å^2$
C6a	286.2 $Å^2$	116 $Å^2$	106 $Å^2$
C6b	220.5 $Å^2$	177.6 $Å^2$	135.8 $Å^2$

3.4 Confocal microscopy imaging

Confocal microscopy imaging of C6a and C6b was carried out in MLVs of different DOPC/DOPG compositions. To evaluate C6a and C6b behaviour in

MLVs characterized by different membrane charge we used MLVs composed of zwitterionic DOPC, negatively charged DOPG and DOPC/DOPG varying in composition (90:10; 60:40; 40:60; 10:90 M/M). The peptides were labelled with NBD fluorophore[4] to examine their localization on the vesicles. MLVs were imaged alone and in presence of the labelled peptides. (Figures 7 and 8) In absence of peptide, MLVs assume spherical shape, with diameter ranging from 5 to 20 µm; addition of C6a NBD^{773}-Trp and C6b NBD^{770}-Trp induces fluorescence of lipid membranes, indicating the localization of the peptides on the lipid surface. Figures 7-8 report confocal microscopy images of MLVs composed of DOPC/DOPG 90:10 M/M, in presence of NBD-labelled C8, C6a and C6b peptides.

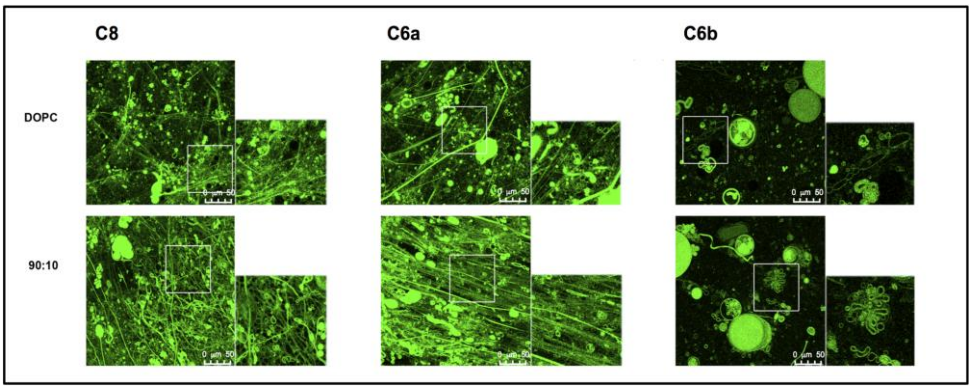

Figure 7. Confocal microscopy images of MLVs in presence of NBD-labeled C8, C6a and C6b peptides. MLVs are composed of DOPC/DOPG 90:10 M/M. Images were acquired on a laser scanning confocal microscope (LSM 510; Carl Zeiss MicroImaging) equipped with a plan Apo 63X, NA 1.4 oil immersion objective lens. For each field, both fluorescent and transmitted light images were acquired on separate photomultipliers and were analysed with Zeiss LSM 510 4.0 SP2 software.

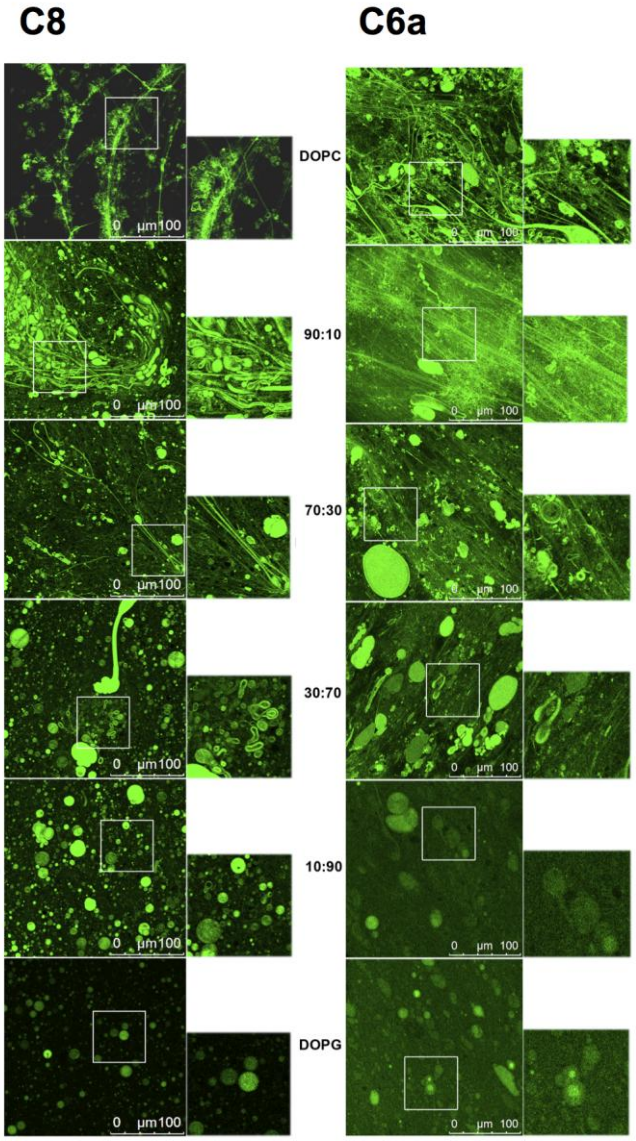

Figure 8. Confocal microscopy images of MLVs in presence of NBD labeled C8 (left) and C6a (right) peptides. MLVs vary in DOPC/DOPG composition moving from DOPC/DOPG 100:0 M/M (top) to DOPC/DOPG 0:100 M/M (bottom). Images were acquired on a laser scanning confocal microscope (LSM 510; Carl Zeiss MicroImaging) equipped with a plan Apo 63X, NA 1.4 oil immersion objective lens. For each field, both fluorescent and transmitted light images were acquired on separate photomultipliers and were analysed with Zeiss LSM 510 4.0 SP2 software.

Figure 7 shows that in MLVs composed of DOPC/DOPG 90:10 M/M and including C6b, the diameter ranges between 5 and 10 µm; only sporadically membrane fusion occurs, generating MLVs up to 50 µm diameter. In presence of C6a peptide highly dynamic budding and fusion events are observable: large spherical liposomes characterized by 5-20 µM diameter often appear because of the impaired budding of the smaller vesicles. Notably, MLVs are interconnected through the formation of straight-chain tubular structures that often extend throughout the entire field of view and beyond and are typically capped at both ends with large liposomal structures. These "tubulation" events occur in different z-planes, forming a crowded three-dimensional network of tubules and liposomes.

The frequency of tubule formation is high in DOPC and 90:10 DOPC/DOPG M/M samples and decreases with the reduction of DOPC concentration, until nearly disappearing in the DOPC/DOPG 10:90 M/M and fully DOPG samples. A similar pattern of tubulation and budding is shown by MLVs in presence of C8 peptide (Figures 7 and 8), indicating that the residues Asp^{772}-Ile^{777}, corresponding to the C6a sequence, have the structural requirements necessary to the membrane active property.

Discussion

Antiviral activity of Trp rich peptide C8 is related to its membrane binding properties, with a major role of Trp residues. SAR studies on C8 resulted in the synthesis of C6a and C6b, two shorter C8 derivatives resulting from the truncation of ^{770}Trp-Glu^{771} and ^{776}Trp-Ile^{777} residues respectively. C6a and C6b, although very similar in their aminoacid composition, differing by only one residue and including two of the three Trp present in C8, are different for their anti-FIV activity. To investigate the conformational factors that in C6a and C6b are

responsible for different biological effects, we studied the conformation of the peptides in DPC/SDS micelle solutions using CD and NMR spectroscopy. On a higher macroscopic scale, we analysed the effect of the two peptides on the membrane surface, using confocal microscopy in MLVs of different DOPC/DOPG compositions. Confirmation of the relationship between antiviral activity and membrane binding resulted from the confocal microscopy imaging. NBD-labeled C6b, which is inactive as an antiviral, appears localized on the surface of DOPC/DOPG MLVs, leaving the surface nearly unaltered; in contrast the NBD-labeled C6a similar to C8 perturbs the surface of the vesicles, modifying vesicle size and inducing membrane "nipples" and membrane tubes. Figure 8 shows a comparison of confocal microscopy images of MLVs with different DOPC/DOPG compositions, including either C6a or C8. C6a and C8 both induce membrane tubulation in a manner dependent on the DOPC/DOPG composition. In MLVs characterized by a zwitterionic phospholipid content less than 50%, the effect of C6a is an increase of vesicle size possibly consequent to vesicle fusion. In contrast, in MLVs having a zwitterionic phospholipid content more than 50% (or in pure DOPC vesicles), C6a induces membrane deformation with the development of a complex network of membrane tubes. The ability of C6a and C8 to induce membrane tubulation and vesicle deformation appears to correlate with their antiviral properties, providing evidence for a mechanism of antiviral activity based on membrane binding property. Interestingly, our data point to the physical-chemical properties of phospholipid bilayer as determinant for the peptide final effect on the membrane architecture: this aspect is important and should not be underestimated when considering the risk for virus resistance.

As previously reported, the conformations of C6a and C6b were studied in mixed zwitterionic DPC/SDS (90:10 M/M) micelles. Both of the peptides assume

well-structured conformation in the micelle solution. This may be explained considering that the peptides are confined to the surface of micelles and have limited conformational freedom. Analysis of the backbone dihedral angles reveals that C6a adopts a regular β-turn structure involving the residues Trp^{773}-Trp^{776}, while C6b assumes folded, but irregular, secondary structures. According to the aminoacid sequences, we can infer that in C6a, the ^{774}Val-Gly^{775} residues act as a flexible linker between Trp^{773} and Trp^{776}, favouring a regular β-turn conformation. In C6b, ^{771}Glu-Asp^{772} residues form a more rigid linker between Trp^{770} and Trp^{773}, preventing the formation of more regular secondary structures. The C6a and C6b NMR models evidence that the prevalent C6a conformer is characterized by an elongated molecular shape, with the indole rings of Trp^{773} and Trp^{776} in a nearly parallel orientation. These generate a hydrophobic molecular surface of 220.5 $Å^2$. The negatively charged Asp^{772} side chain flanks the Trp^{773} indole ring directly in this molecular area.

Contrarily to C6a, C6b has a globular shape and the molecular surface generated by these residues is smaller as compared to C6a. The negatively charged side chains of Glu^{771} and Asp^{772} are on the direct opposite side with respect to the Trp indole rings.

Many peptides have been studied as antiviral fusion inhibitors. However, those approved for antiviral therapy have large dimensions with considerable problems deriving from the high cost and the difficulty of administration. C8 and its derivatives have the advantage of being small peptides. The structural data obtained from our study make it possible to identify a pharmacophore model from which to design new small peptide-peptidomimetic molecules. The comparison of the most representative conformations of C8 and C6a indicates that it is possible to identify a common pharmacophore profile represented by two indole rings,

which in C8 belong to Trp^{770} and Trp^{776} and the side chain of Asp^{772}, while in C6a belong to Trp^{773} and Trp^{776} and the side chain of Asp^{772}. These three functional groups maintain similar distances in the two peptides.

Taken together our data show that synergic molecular interactions involving surfaces of Trp and side chain of Asp residue result in the destabilization of the bilayer organization, membrane surface deformation and membrane tube formation; these common membrane destabilizing properties of C6a and C8, define the structural basis of their antiviral activity.

Conclusions

C6a and C6b, two derivatives of the C8 anti-FIV peptide, although very similar to their precursor show different activity profile: in particular, C6a preserves anti-viral activity, while C6b is nearly inactive. We analysed C6a and C6b in bio-membrane mimicking environments using CD and NMR spectroscopy and confocal microscopy. Our data provide additional evidence that common antiviral activity profiles correspond to similar membrane binding properties: actually C6a, similarly to C8, has the ability to destabilize membrane vesicles, producing complex network of membrane tubes. Conformational data show that the action of C6a and C8 at membrane level is mediated by interactions involving Asp^{772} and two Trp residues, which correspond to Trp^{770} and Trp^{776} in C8, and Trp^{773} and Trp^{776} in C6a. These residues define a pharmacophoric model that can be considered the basis to design simplified molecules, overcoming the pharmacokinetic and high cost limitations affecting the entry inhibitors currently used as anti-HIV drugs.

References

1. D'Ursi, A. M.; Giannecchini, S.; Esposito, C.; Alcaro, M. C.; Sichi, O.; Armenante, M. R.; Carotenuto, A.; Papini, A. M.; Bendinelli, M.; Rovero, P. Development of antiviral fusion inhibitors: short modified peptides derived from the transmembrane glycoprotein of feline immunodeficiency virus. *Chembiochem* **2006,** 7, 774-9.

2. Giannecchini, S.; Di Fenza, A.; D'Ursi, A. M.; Matteucci, D.; Rovero, P.; Bendinelli, M. Antiviral activity and conformational features of an octapeptide derived from the membrane-proximal ectodomain of the feline immunodeficiency virus transmembrane glycoprotein. *J. Virol.* **2003,** 77, 3724-33.

3. D'Errico, G.; Vitiello, G.; D'Ursi, A. M.; Marsh, D. Interaction of short modified peptides deriving from glycoprotein gp36 of feline immunodeficiency virus with phospholipid membranes. *Eur. Biophys J.* **2009,** 38, 873-82.

4. Dufau, I.; Mazarguil, H. Design of a fluorescent amino acid derivative usable in peptide synthesis. *Tetrahedron Letter.* **2000,** 41, 6063-6066.

5. Yi, H. A.; Fochtman, B. C.; Rizzo, R. C.; Jacobs, A. Inhibition of HIV Entry by Targeting the Envelope Transmembrane Subunit gp41. *Curr. HIV Res.* **2016,** 14, 283-94.

6. Zerbe, O. BioNMR in drug research methods and principles in medicinal chemistry. **2003**.

7. Whitmore, L.; Wallace, B. A. DICHROWEB, an online server for protein secondary structure analyses from circular dichroism spectroscopic data. *Nucleic Acids Res.* **2004,** 32, W668-73.

8. Wüthrich, K. NMR with Proteins and Nucleic Acids. *Europhys. News* **1986,** 17, 11-13.

9. Goddard, T.; Kneller, D. SPARKY 3. *University of California, San Francisco* **2004**.

10. Guntert, P. Automated NMR structure calculation with CYANA. *Methods Mol. Biol.* **2004,** 278, 353-78.

11. Hutchinson, E. G.; Thornton, J. M. PROMOTIF--a program to identify and analyze structural motifs in proteins. *Protein Sci* **1996,** 5, 212-20.

12. Merlino, A.; Vitiello, G.; Grimaldi, M.; Sica, F.; Busi, E.; Basosi, R.; D'Ursi, A. M.; Fragneto, G.; Paduano, L.; D'Errico, G. Destabilization of lipid membranes by a peptide derived from glycoprotein gp36 of feline immunodeficiency virus: a combined molecular dynamics/experimental study. *J. Phys. Chem. B* **2012,** 116, 401-12.

13. Rizvi, S. M.; Shakil, S.; Haneef, M. A simple click by click protocol to perform docking: AutoDock 4.2 made easy for non-bioinformaticians. *EXCLI J.* **2013,** 12, 831-57.

4 Investigating interaction of gp36-MPER with membrane models

MPER, known as the membrane proximal external region, is a ~24-residue hydrophobic region (residues 660–683), immediately preceding the transmembrane domain (TM) and is one of the most conserved regions in lentivirus glycoproteins.

MPER is rich in aromatic, particularly Trp, residues and shows a marked tendency to remain permanently at membrane interface, determining the destabilization of the double layer structure on the membrane of the target cell. Many studies have shown that deletion or substitution of this region changes the fusogenic effects of viral glycoproteins and the entry of the virus into the host cell.[1] In fact, mutations of the first three Trp (Trp^{666}, Trp^{670}, Trp^{672}) of gp41 are sufficient to prevent viral fusion.

MPER is the epitope for several well-characterized broadly neutralizing antibodies, therefore it is currently receiving increasing attention as potential targets for vaccine development.[2-5] Furthermore, similarly to NHR and CHR, MPER is an attractive target to design new molecules preventing the correct positioning of the viral glycoproteins with the host cell membrane.[6-23]

gp41-MPER structure has been extensively studied by both NMR and X-ray crystallography under a wide range of conditions,[24-29] indicating the prevalence of two α-helical regions connected by a sharp turn. In this framework, the polypeptide corresponding to the sequence Leu^{737}-Met^{785} of

gp36 (gp36-CHR-MPER) and including the CHR and the MPER regions of gp36, was previously cloned, expressed and purified in the lab where I worked for my PhD project. The NMR structure of the ^{15}N and ^{13}C labelled protein was previously solved using 2D and 3D homo and hetero nuclear techniques.

To characterize interaction of gp36-CHR-MPER with lipid surface, part of my research activity was focused on the NMR studies of gp36-CHR-MPER in presence of paramagnetic spin probes. Additionally, gp36-CHR-MPER was analyzed by confocal microscopy imaging in presence of DOPC/DOPG MLVs. Data coming from the mentioned analyses are discussed in comparison with those previously obtained on C8 and its shorter derivatives.[30]

4.1 gp36-CHR-MPER NMR structure

The NMR structure of isotope labelled gp36-CHR-MPER was previously studied in our lab in mixed DPC/SDS (90:10 M/M) micelles.[31-33] NMR spectra of (^{15}N-^{13}C)-labelled gp36-CHR-MPER in mixed DPC/SDS (90:10 M/M) micelles were recorded on 900MHz Bruker Avance III spectrometer using 2D and 3D homo and hetero nuclear experiments on (^{15}N-^{13}C)-labelled gp36-CHR-MPER[34] (PDB ID: 6FTK).

Part of my research activity was aimed at the refinement of NMR structure preliminary obtained with CYANA software on the basis of NOEs data. Accordingly, structure was refined using TALOS+ software[35] integrating, as input file for structure calculation, backbone dihedral restraints derived from chemical shifts values. NMR structure bundle (Figure 1) including 10 gp36-CHR-MPER NMR conformers, evidences good definition on Glu^{748}-Gly^{778} fragment (RMSD backbone heavy atoms: 1.10Å). Analysis of backbone dihedral angles according to PROMOTIF algorithm[36] points to the presence of

i) α-helix on Thr^{739}-Tyr^{747} residues, ii) 3,10-helix on Glu^{748}-Gly^{760} and Gln^{765}-Leu^{784} residues, iii) type II β-turn on Lys^{761}-Ile^{764} residues.

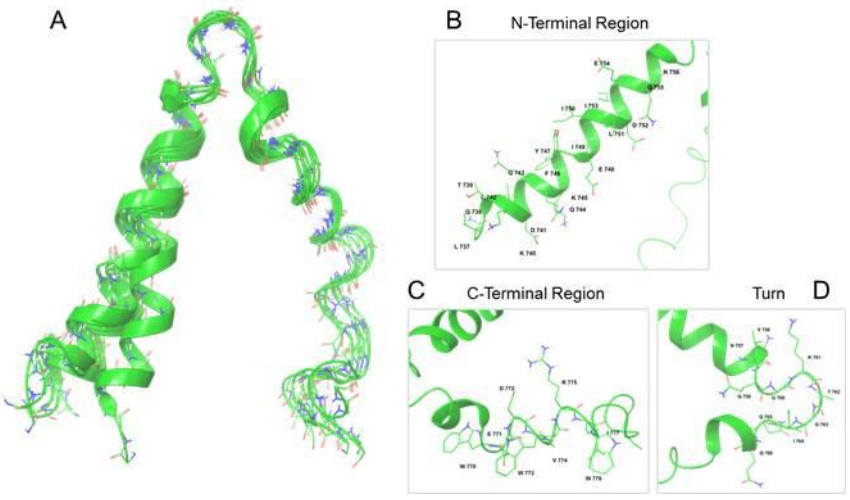

Figure 1. NMR structure of (^{15}N-^{13}C)-labelled gp36-CHR-MPER in DPC/SDS 90:10 M/M. A) Ribbon representation of the average structure of the calculated ensemble; B) N-terminal region consisting of α-helix on Gln^{738}-Asn^{756} residues; C) C-terminal region containing the C8 peptide; D) Turn region containing Val^{758}–Gln^{765} residues.

4.1.1 NMR spin-label analysis

NMR analysis in DPC/SDS 90:10 M/M micelle solutions, was the starting point to investigate the positioning of gp36-CHR-MPER with respect to the micelle aggregates. To this end, we recorded 2D ^{15}N-HSQC spectra of (^{15}N-^{13}C)-labelled gp36-CHR-MPER in DPC/SDS 90:10 M/M micelle solutions in absence and in presence of 5-DSA.[37] ^{15}N-NHQC spectra of ^{15}N-labelled gp36-CHR-MPER evidence dramatic changes in backbone NH intensities relative to Leu^{767}, Gln^{768}, Trp^{776}, Gly^{778} and Ile^{780}. Several other residues show less consistent perturbation upon 5-DSA addition (Figure 2).

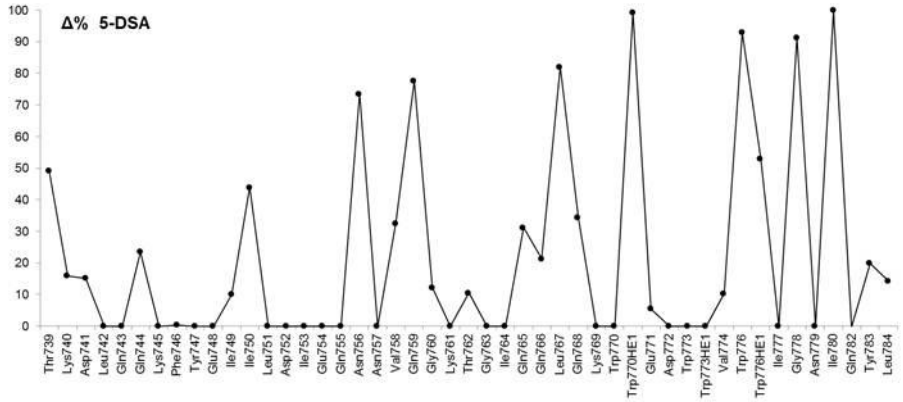

Figure 2. Percentage variation (Δ%) of intensities of HN backbone peaks of (^{15}N-^{13}C)-labelled gp36-CHR-MPER in DPC/SDS 90:10 M/M micelle solutions obtained by integrating 2D ^{15}N-HSQC spectra recorded at 300 K in absence and in presence of 5-DSA at a concentration of one spin label *per* micelle.

The rationalization of these data, using Maestro software[38] allow for the description of a model of exposition of gp36-CHR-MPER to the phospholipid micelles as reported in Figure 3.

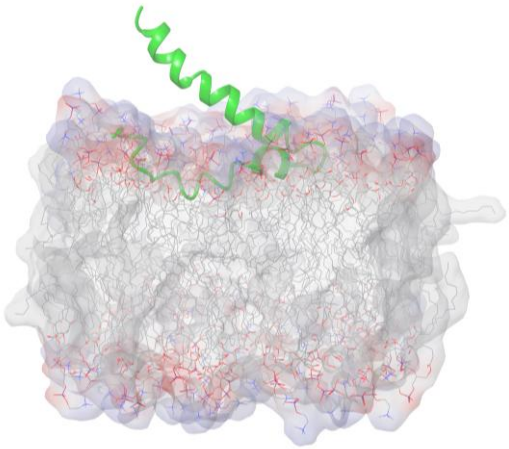

Figure 3. Interaction model of gp36-CHR-MPER (in green) exposition to the phospholipid micelles.

4.2 Confocal microscopy imaging

Confocal microscopy imaging of gp36-CHR-MPER was carried out in labelled MLVs of DOPC/DOPG 90:10 M/M. To evaluate the behavior of MPER in MLVs, we used labelled MLVs composed of zwitterionic DOPC and negatively charged DOPG. DOPC included 10% of NBD-PC (1-palmitoyl-2-{6-[(7-nitro-2-1,3-benzoxadiazol-4-yl) amino] hexanoyl}-sn glycero-3-phosphocholine) for fluorescence visualization. Labelled MLVs were imaged alone and in presence of gp36-CHR-MPER. (Figure 4) Figure 4A reports confocal microscopy images of MLVs composed of DOPC/DOPG 90:10 M/M, in absence of gp36-CHR-MPER. In these conditions, labelled MLVs assume spherical shape, with diameter ranging from ~1 to 10 µm.

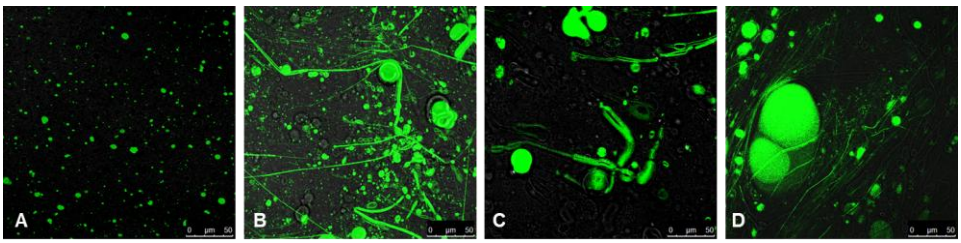

Figure 4. A Confocal microscopy images of labelled MLVs in absence of gp36-CHR-MPER and B, C and D in presence of gp36-CHR-MPER. Labelled MLVs are composed of DOPC/DOPG 90:10 M/M. DOPC amount is characterized of 10% of NBD-PC. Images were acquired on a laser scanning confocal microscope (LSM 510; Carl Zeiss MicroImaging) equipped with a plan Apo 63X, NA 1.4 oil immersion objective lens. For each field, both fluorescent and transmitted light images were acquired on separate photomultipliers and were analyzed with Zeiss LSM 510 4.0 SP2 software.

Figures 4 B, C and D show that in fluorescent labelled MLVs composed of DOPC/DOPG 90:10 M/M with 10% of NBD-PC and including gp36-CHR-

MPER, the diameter of vesicles increases due to highly dynamic budding and fusion events. Large spherical liposomes characterized by 5-30 µm diameter often appear because of the impaired budding of the smaller vesicles. Notably, labelled MLVs are interconnected through the formation of straight-chain tubular structures (Figure 4 B, C and D) that often extend throughout the entire field of view and beyond and are typically capped at both ends with large liposomal structures. These "tubulation" events occur in different z-planes, forming a crowded three dimensional network of tubules and liposomes.

4.2.1 Confocal microscopy imaging on HeLa cellular vesicles

In an attempt to work on even more biomimetic systems, we performed confocal microscopy imaging of gp36-CHR-MPER and its derivatives C8 and C6a on plasma membrane-derived vesicles, which bud off cells in response to external stress.[39, 40] These vesicles are derived from the native *HeLa* cellular membranes and are thus more native-like than vesicles made of synthetic lipids. Our cellular vesicles were produced using vesiculation method, utilizing the chemicals formaldehyde and dithiothreitol (DTT) to stress the cells and to induce an apoptosis-like response.[39, 41, 42]

To observe fluorescence for C8 and C6a in *HeLa* cellular membranes, we used 0.5mM NBD-labelled C8 and 0.5mM NBD-labelled C6a peptides, while to observe fluorescence for gp36-CHR-MPER in the same conditions, we used NBD-PC 1% (1-palmitoyl-2-{6-[(7-nitro-2-1,3-benzoxadiazol-4-yl) amino] hexanoyl}-sn-glycero-3-phosphocholine) and 0.05mM MPER. In absence of MPER, *HeLa* cellular vesicles assume spherical shape, with diameter ranging from 100 nm to 1 µm. Figure 5A report confocal microscopy images of cellular vesicles in absence of peptides. Figures 5B-C show that NBD-labelled

gp36-CHR-MPER, C8 and C6a induce increasing motion of cellular vesicles to reach an aligned position. In this step, we supposed to be preliminary to vesicle fusion, formation of thin straight-chain tubular structures and membrane filaments occur, as observed for DOPC/DOPG vesicles.

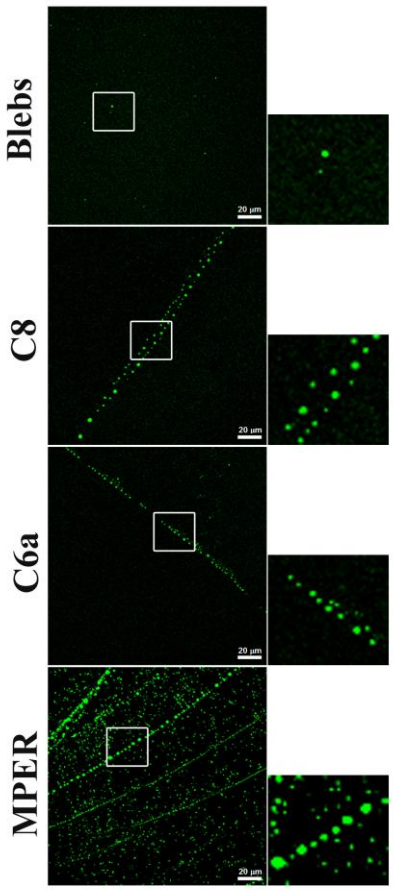

Figure 5. A Blebs in absence of labelled peptides. B Confocal microscopy imaging of blebs in presence of 0.5mM NBD-labelled C8 peptide. C Confocal microscopy imaging of blebs in presence of 0.5mM NBD-labelled C6a peptide. D Confocal microscopy imaging of blebs in presence of NBD-PC and 0.05mM MPER.

Discussion

As previously reported, NMR structure of gp36-CHR-MPER consists of i) α-helix on Thr^{739}-Tyr^{747} residues, ii) 3,10-helix on Glu^{748}-Gly^{760} and Gln^{765}-Leu^{784} residues, iii) type II β-turn on Lys^{761}-Ile^{764} residues. Looking at the structural organization of gp36-CHR-MPER, the first observation is that the secondary structure of CHR is more regular as compared to MPER. The structural features of CHR and MPER regions account for their biological roles, that for CHR is the participation to the coiled-coil helix to form the six-helix bundle with NHR region, while for MPER is the binding to the lipid membranes. Indeed, being the binding of MPER with lipid surface non-specific, is tolerant for more disordered structure.

To investigate the factors regulating interaction of MPER with lipid membrane, we analyzed the exposure of gp36-CHR-MPER to the micelle surface using paramagnetic probes. Data collected in presence of 5-DSA showed perturbation of MPER region with strong participation of Trp^{770} and Trp^{777} (Figure 2). Interestingly, Trp^{773} was almost unaffected by 5-DSA, thus indicating an exposition to the aqueous environment.[38] Comparison of these data with those deriving from similar analyses on C8 shows different orientation of Trp residues on membrane surface: in particular, Trp^{770} and Trp^{773} in gp36-CHR-MPER, instead of Trp^{770} and Trp^{776} in C8 are those embedded in the external lipid leaflet.

To interpret these results that apparently contradict the correlation between the position of Trp in the peptide sequence and their role in the interaction with membrane surface, we analyzed the gp36-CHR-MPER molecular surfaces[30] according to the aptitude to engage electrostatic/polar interaction with positively/negatively charged surfaces, or hydrophobic interactions with hydrophobic surfaces.[43] According to this analysis gp36-CHR-MPER and C8

expose 452.9 $Å^2$ and 288.3 $Å^2$ hydrophobic surfaces respectively. The extension of C8 surface is very similar to that calculated for C6a, the shorter derivative exerting biophysical and biological activity similar to C8[30] (Figure 6). Therefore these data suggest a correlation between the extension of hydrophobic surface generated by the indole rings of Trp residues and the aptitude of the peptide fragment to interact with lipid surface.[29]

In our previous characterization of C8 and its derivatives C6a and C6b, we defined a pharmacophore model including the indole rings of the two Trp residues (which in C8 belong to Trp^{770} and Trp^{776}, and in C6a belong to Trp^{773} and Trp^{776}) and the side chain of Asp^{772}. This model fits with the structural features of gp36-CHR-MPER and is consistent with its membrane binding affinity. Therefore, our data support the validity of the pharmacophore to predict an optimized interaction for an efficacy membrane binding activity.

To test the effectiveness of gp36-CHR-MPER on lipid membrane we acquired confocal microscopy data. The microscopy imaging using DOPC/DOPG vesicles shows that gp36-CHR-MPER induces a strong perturbation of the bilayer architecture and consequent modification of size and shape of DOPC/DOPG vesicles (90:10 M/M). Comparison of confocal microscopy data acquired for gp36-CHR-MPER with those previously acquired for C8 and C6a show that all these peptides induce membrane deformation, with the appearance of a complex network of membrane tubes. Confocal microscopy imaging using different concentration of peptides shows that gp36-CHR-MPER is active at tenfold lower concentration, indicating a stronger membrane active property as compared to C8 and C6a and confirming once more a good correlation between the extension of hydrophobic surface and the membrane active property. Finally, we demonstrated that activity of gp36-CHR-MPER and its derivatives on lipid

micelles and vesicles is observable even on *HeLa* cellular vesicles. Data collected with confocal microscopy indicate that gp36-CHR-MPER and its derivatives are active on cellular membrane and their impact on size and shape of the vesicles is not a biophysical artefact, but a real biological activity.

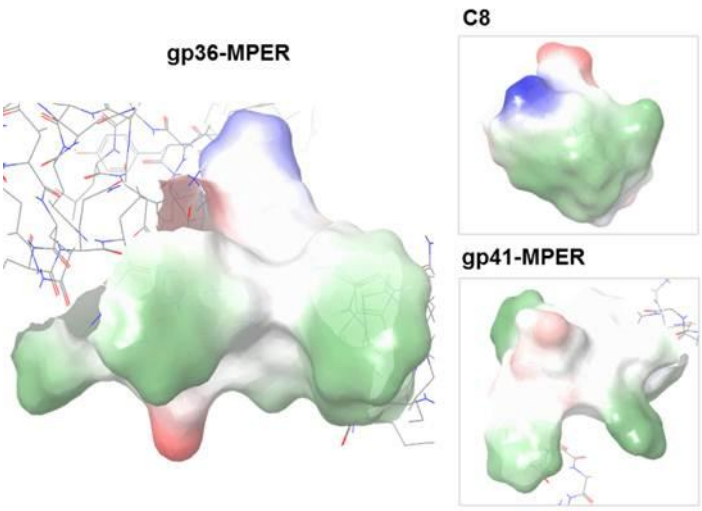

Peptide	Hydrophobic surface	Negative surface	Positive surface
C8	288.3 Å²	210.8 Å²	137.9 Å²
gp36-MPER	377.6 Å²	150.2 Å²	84.3 Å²
gp41-MPER	452.9 Å²	63.7 Å²	20.0 Å²

Figure 6. Comparison between molecular surface of gp36-CHR-MPER (PDB ID: 6FTK), C8 peptide in DPC/SDS 90:10 M/M[30] and gp41-MPER in DMPC/DHPC bicelles (PDB ID: 6E8W),[29] calculated as propensities of the molecules different portions to interact according to the specific surface properties. Molecular surfaces of residues (in green-white) account for the protein propensity to engage hydrophobic interactions. Molecular surfaces of residues (in blue) account for the protein propensity to engage polar/electrostatic interactions.

References

1. Muñoz-Barroso, I.; Salzwedel, K.; Hunter, E.; Blumenthal, R. Role of the membrane-proximal domain in the initial stages of human immunodeficiency virus type 1 envelope glycoprotein-mediated membrane fusion. *Journal of virology* **1999,** 73, 6089-6092.

2. Muster, T.; Steindl, F.; Purtscher, M.; Trkola, A.; Klima, A.; Himmler, G.; Rüker, F.; Katinger, H. A conserved neutralizing epitope on gp41 of human immunodeficiency virus type 1. *Journal of virology* **1993,** 67, 6642-6647.

3. Stiegler, G.; Kunert, R.; Purtscher, M.; Wolbank, S.; Voglauer, R.; Steindl, F.; Katinger, H. A potent cross-clade neutralizing human monoclonal antibody against a novel epitope on gp41 of human immunodeficiency virus type 1. *AIDS research and human retroviruses* **2001,** 17, 1757-1765.

4. Huang, J.; Ofek, G.; Laub, L.; Louder, M. K.; Doria-Rose, N. A.; Longo, N. S.; Imamichi, H.; Bailer, R. T.; Chakrabarti, B.; Sharma, S. K. Broad and potent neutralization of HIV-1 by a gp41-specific human antibody. *Nature* **2012,** 491, 406.

5. Williams, L. D.; Ofek, G.; Schätzle, S.; McDaniel, J. R.; Lu, X.; Nicely, N. I.; Wu, L.; Lougheed, C. S.; Bradley, T.; Louder, M. K. Potent and broad HIV-neutralizing antibodies in memory B cells and plasma. *Science immunology* **2017,** 2.

6. Liu, J.; Deng, Y.; Li, Q.; Dey, A. K.; Moore, J. P.; Lu, M. Role of a Putative gp41 Dimerization Domain in Human Immunodeficiency Virus Type 1 Membrane Fusion. *Journal of Virology* **2010,** 84, 201-209.

7. Muench, J.; Staendker, L.; Adermann, K.; Schuz, A.; Schindler, M.; Chinnadurai, R.; Poehlmann, S.; Chaipan, C.; Biet, T.; Peters, T.; Meyer, B.; Wilhelm, D.; Lu, H.; Jing, W.; Jiang, S.; Forssmann, W.-G.; Kirchhoff, F. Discovery and optimization of a natural HIV-1 entry inhibitor targeting the gp41 fusion peptide. *Cell* **2007,** 129, 263-275.

8. Suarez, T.; Nir, S.; Goni, F. M.; Saez-Cirion, A.; Nieva, J. L. The pre-transmembrane region of the human immunodeficiency virus type-1 glycoprotein: a novel fusogenic sequence. *Febs Letters* **2000,** 477, 145-149.

9. Suarez, T.; Gallaher, W. R.; Agirre, A.; Goni, F. M.; Nieva, J. L. Membrane interface-interacting sequences within the ectodomain of the human immunodeficiency virus type 1 envelope glycoprotein: Putative role during viral fusion. *Journal of Virology* **2000,** 74, 8038-8047.

10. Salzwedel, K.; West, J. T.; Hunter, E. A conserved tryptophan-rich motif in the membrane-proximal region of the human immunodeficiency virus type 1 gp41 ectodomain is important for Env-mediated fusion and virus infectivity. *Journal of Virology* **1999,** 73, 2469-2480.

11. Schibli, D. J.; Montelaro, R. C.; Vogel, H. J. The membrane-proximal tryptophan-rich region of the HIV glycoprotein, gp41, forms a well-defined helix in dodecylphosphocholine micelles. *Biochemistry* **2001,** 40, 9570-9578.

12. Ji, H.; Shu, W.; Burling, F. T.; Jiang, S. B.; Lu, M. Inhibition of human immunodeficiency virus type 1 infectivity by the gp41 core: Role of a conserved hydrophobic cavity in membrane fusion. *Journal of Virology* **1999,** 73, 8578-8586.

13. Judice, J. K.; Tom, J. Y. K.; Huang, W.; Wrin, T.; Vennari, J.; Petropoulos, C. J.; McDowell, R. S. Inhibition of HIV type 1 infectivity by constrained alpha-helical peptides: Implications for the viral fusion mechanism. *Proceedings of the National Academy of Sciences of the United States of America* **1997,** 94, 13426-13430.

14. Wild, C. T.; Shugars, D. C.; Greenwell, T. K.; McDanal, C. B.; Matthews, T. J. Peptides corresponding to a predictive alpha-helical domain of human-immunodeficiency-

virus type-1 gp41 are potent inhibitors of virus-infection. *Proceedings of the National Academy of Sciences of the United States of America* **1994,** 91, 9770-9774.

15. Neurath, A. R.; Strick, N.; Lin, K.; Jiang, S. Multifaceted consequences of anti-gp41 monoclonal-antibody 2F5 binding to hiv type-1 virions. *Aids Research and Human Retroviruses* **1995,** 11, 687-696.

16. Kilby, J. M.; Lalezari, J. P.; Eron, J. J.; Carlson, M.; Cohen, C.; Arduino, R. C.; Goodgame, J. C.; Gallant, J. E.; Volberding, P.; Murphy, R. L.; Valentine, F.; Saag, M. S.; Nelson, E. L.; Sista, P. R.; Dusek, A. The safety, plasma pharmacokinetics, and antiviral activity of subcutaneous enfuvirtide (T-20), a peptide inhibitor of gp41-mediated virus fusion, in HIV-infected adults. *Aids Research and Human Retroviruses* **2002,** 18, 685-693.

17. Lazzarin, A.; Clotet, B.; Cooper, D.; Reynes, J.; Arasteh, K.; Nelson, M.; Katlama, C.; Stellbrink, H.-J.; Delfraissy, J.-F.; Lange, J. Efficacy of enfuvirtide in patients infected with drug-resistant HIV-1 in Europe and Australia. *New England Journal of Medicine* **2003,** 348, 2186-2195.

18. Barbato, G.; Bianchi, E.; Ingallinella, P.; Hurni, W. H.; Miller, M. D.; Cilibertol, G.; Cortese, R.; Bazzo, R.; Shiver, J. W.; Pessi, A. Structural analysis of the epitope of the Anti-HIV antibody 2F5 sheds light into its mechanism of neutralization and HIV fusion. *Journal of Molecular Biology* **2003,** 330, 1101-1115.

19. Giannecchini, S.; Di Fenza, A.; D'Ursi, A. M.; Matteucci, D.; Rovero, P.; Bendinelli, M. Antiviral activity and conformational features of an octapeptide derived from the membrane-proximal ectodomain of the feline immunodeficiency virus transmembrane glycoprotein. *Journal of virology* **2003,** 77, 3724-3733.

20. Jiang, S.; Lin, K.; Strick, N.; Neurath, A. R. Inhibition of HIV-1 infection by a fusion domain binding peptide from the HIV-1 envelope glycoprotein GP41. *Biochemical and biophysical research communications* **1993,** 195, 533-538.

21. Jin, B.-S.; Ryu, J.-R.; Ahn, K.; Yu, Y. G. Design of a peptide inhibitor that blocks the cell fusion mediated by glycoprotein 41 of human immunodeficiency virus type 1. *AIDS research and human retroviruses* **2000,** 16, 1797-1804.

22. Kilby, J. M.; Eron, J. J. Novel therapies based on mechanisms of HIV-1 cell entry. *New England Journal of Medicine* **2003,** 348, 2228-2238.

23. Massi, C.; Indino, E.; Lami, C.; Fissi, A.; Pieroni, O.; La Rosa, C.; Esposito, F.; Galoppini, C.; Rovero, P.; Bandecchi, P. The antiviral activity of a synthetic peptide derived from the envelope SU glycoprotein of feline immunodeficiency virus maps in correspondence of an amphipathic helical segment. *Biochemical and biophysical research communications* **1998,** 246, 160-165.

24. Sun, Z.-Y. J.; Oh, K. J.; Kim, M.; Yu, J.; Brusic, V.; Song, L.; Qiao, Z.; Wang, J.-h.; Wagner, G.; Reinherz, E. L. HIV-1 broadly neutralizing antibody extracts its epitope from a kinked gp41 ectodomain region on the viral membrane. *Immunity* **2008,** 28, 52-63.

25. Kim, M.; Sun, Z.-Y. J.; Rand, K. D.; Shi, X.; Song, L.; Cheng, Y.; Fahmy, A. F.; Majumdar, S.; Ofek, G.; Yang, Y. Antibody mechanics on a membrane-bound HIV segment essential for GP41-targeted viral neutralization. *Nature structural & molecular biology* **2011,** 18, 1235.

26. Liu, J.; Deng, Y.; Dey, A. K.; Moore, J. P.; Lu, M. Structure of the HIV-1 gp41 membrane-proximal ectodomain region in a putative prefusion conformation. *Biochemistry* **2009,** 48, 2915-2923.

27. Buzon, V.; Natrajan, G.; Schibli, D.; Campelo, F.; Kozlov, M. M.; Weissenhorn, W. Crystal structure of HIV-1 gp41 including both fusion peptide and membrane proximal external regions. *PLoS pathogens* **2010,** 6, e1000880.

28. Shi, W.; Bohon, J.; Han, D.; Habte, H.; Qin, Y.; Cho, M. W.; Chance, M. R. Structural characterization of HIV GP41 with the membrane proximal external region. *Journal of Biological Chemistry* **2010**, jbc. M110. 111351.

29. Fu, Q.; Shaik, M. M.; Cai, Y.; Ghantous, F.; Piai, A.; Peng, H.; Rits-Volloch, S.; Liu, Z.; Harrison, S. C.; Seaman, M. S. Structure of the membrane proximal external region of HIV-1 envelope glycoprotein. *Proceedings of the National Academy of Sciences* **2018,** 115, E8892-E8899.

30. Grimaldi, M.; Stillitano, I.; Amodio, G.; Santoro, A.; Buonocore, M.; Moltedo, O.; Remondelli, P.; D'Ursi, A. M. Structural basis of antiviral activity of peptides from MPER of FIV gp36. *PLoS One* **2018,** 13, e0204042.

31. Weller, K.; Lauber, S.; Lerch, M.; Renaud, A.; Merkle, H.; Zerbe, O. Biophysical and biological studies of end-group-modified derivatives of Pep-1. *Biochemistry* **2005,** 44, 15799-15811.

32. Pandey, S.; Alcaro, M. C.; Scrima, M.; Peroni, E.; Paolini, I.; Di Marino, S.; Barbetti, F.; Carotenuto, A.; Novellino, E.; Papini, A. M.; D'Ursi, A. M.; Rovero, P. Designed glucopeptides mimetics of myelin protein epitopes as synthetic probes for the detection of autoantibodies, biomarkers of multiple sclerosis. *J Med Chem* **2012,** 55, 10437-47.

33. Mannhold, R.; Kubinyi, H.; Folkers, G.; Zerbe, O. *BioNMR in drug research*. John Wiley & Sons: 2006; Vol. 16.

34. Goddard, T.; Kneller, D. SPARKY 3. *University of California, San Francisco* **2004**.

35. Shen, Y.; Delaglio, F.; Cornilescu, G.; Bax, A. TALOS+: a hybrid method for predicting protein backbone torsion angles from NMR chemical shifts. *J Biomol NMR* **2009,** 44, 213-23.

36. Hutchinson, E. G.; Thornton, J. M. PROMOTIF - A program to identify and analyze structural motifs in proteins. *Protein Science* **1996,** 5, 212-220.

37. Zerbe, O. BioNMR in drug research (methods and principles in medicinal chemistry). In Wiley-VCH, Weinheim: 2003.

38. Wizard, P. P.; Maestro, M.; Phase, I. F. Jaguar, and Glide. *Schrödinger, LLC: Portland, OR* **2009**.

39. Scott, R. E. Plasma membrane vesiculation: a new technique for isolation of plasma membranes. *Science* **1976,** 194, 743-745.

40. Del Piccolo, N.; Placone, J.; He, L.; Agudelo, S. C.; Hristova, K. Production of plasma membrane vesicles with chloride salts and their utility as a cell membrane mimetic for biophysical characterization of membrane protein interactions. *Analytical chemistry* **2012,** 84, 8650-8655.

41. Scott, R. E.; Maercklein, P. B. Plasma membrane vesiculation in 3T3 and SV3T3 cells. II. Factors affecting the process of vesiculation. *Journal of Cell Science* **1979,** 35, 245-252.

42. Scott, R. E.; Perkins, R.; Zschunke, M.; Hoerl, B.; Maercklein, P. Plasma membrane vesiculation in 3T3 and SV3T3 cells. I. Morphological and biochemical characterization. *Journal of Cell Science* **1979,** 35, 229-243.

43. Rizvi, S. M.; Shakil, S.; Haneef, M. A simple click by click protocol to perform docking: AutoDock 4.2 made easy for non-bioinformaticians. *EXCLI J.* **2013,** 12, 831-57.

Materials and Methods

Peptide Synthesis

The C8, C6a and C6b peptides were synthesized by the Fmoc solid phase synthesis method according to the previously published procedure.[1] For the confocal microscopy analysis, all peptides labelled with nitrobenzoxadiazole (NBD) fluorophore and the L-diamino propionic acid Fmoc-Dap(NBD)-OH)[2] were used in substitution of ^{770}Trp for C8 and C6b and ^{773}Trp for C6a. Labelled C8 peptide was prepared by synthesizing Ac-^{770}Dap(NBD)EDWVGWI^{777}-NH_2, the C6b peptide was prepared by synthesizing Ac-^{770}Dap(NBD)EDWVG^{775}-NH_2, and the C6a peptide was prepared by synthesizing Ac-^{772}D-Dap(NBD)-VGWI^{777}-NH_2.

CD analysis

CD experiments were performed at 25°C on an 810-Jasco spectropolarimeter as an average of 4 scans with 10 nm/min scan speed, 4 s response time and 2 nm bandwidth, using a quartz cuvette with a path length of 1 mm, a measurement range from 190 to 260 nm (far UV), at temperature of 25°C. Throughout the measurements, the trace of the high tension voltage was verified to be less than 700 V, which ensures the reliability of the obtained data. Far UV CD spectrum of only mixed micelles (DPC/SDS 90:10 M/M (27 mM/3 mM)) in aqueous solution (pH 7.4, 10 mM phosphate buffer containing H_2O) was acquired as reference, than 500 μM of C6a and C6b peptides were added to mixed micelles for the conformational analysis.[3] The processed curves of C6a and C6b peptides in mixed micelles were obtained by using Spectra Analysis tool of Jasco software. The CD

curves of C6a and C6b peptides in mixed micelles were corrected for the solvent contribution by subtraction of CD reference spectrum and then final CD spectra were obtained after baseline correction and binomial smoothing. Those resulting spectra were used for the estimation of the secondary structure content using the algorithms CONTIN and SELCON from the DICHROWEB website.[4]

NMR analysis

***Sample preparation*:** Samples for the NMR experiments were prepared at 1 mM C6a and C6b concentrations, in a mixture of d_{38}-DPC or d_{25}-SDS 90:10 M/M (27 mM/3 mM) in aqueous solution (pH 7.4, 10 mM phosphate buffer containing H_2O/D_2O).[3] For the spin label experiments, the 5- and 16-doxylstearic acids were solubilized in dimethyl sulfoxide-d_6 and then added to the samples.

Spectra acquisition and analysis: NMR spectra were recorded on a Bruker DRX-600 spectrometer. All samples had a recording of the 1D ^{1}H homonuclear spectra in the Fourier mode, with quadrature detection and two-dimensional (2D) TOCSY and NOESY spectra in the phase–sensitive mode using quadrature detection in $\omega 1$ by time–proportional phase incrementation of the initial pulse.[5-7] The water signal was suppressed using WATERGATE pulse sequence experiments.[8]

Data block sizes contained 2048 addresses in t_2 and 512 equidistant t_1 values. Prior to Fourier transformation, the time domain data matrices were multiplied by shifted $\sin^2$ functions in both dimensions. A mixing time of 70 ms was used for the TOCSY experiments. The NOESY experiments were run at 300 K with mixing times in the range of 100-300 ms. Qualitative and quantitative analyses of TOCSY and NOESY spectra were carried out using SPARKY software.[9]

***Structure calculations*.** Peak volumes were translated into upper distance bounds with the CALIBA routine from the CYANA software package.[10] The requisite pseudo-atom corrections were applied for non-stereo specifically assigned protons at prochiral centres and for the methyl group. After discarding redundant and duplicated constraints, the final list of experimental constraints was used to generate a group of 100 structures by the standard CYANA protocol of simulated annealing in the torsion angle space (using 10.000 steps). No dihedral angle or hydrogen bond restraints were applied. The best 20 structures that had low target function values and small residual violations were refined by *in vacuo* minimization in the AMBER 1991 force field using the SANDER program of the AMBER 5.0 suite.[11, 12] In order to mimic the effect of solvent screening, all net charges were reduced to 20% of their true values. Additionally, a distance-dependent dielectric constant ($\varepsilon = r$) was used.

The cut-off for non-bonded interactions was 12 Å. The NMR-derived upper bounds were imposed as semi-parabolic penalty functions, with force constants of 16 Kcal/mol $Å^2$. The function was shifted to be linear when the violation exceeded 0.5 Å. The best 10 structures after minimization had AMBER energies ranging from -441.4 to -391.1 Kcal/mol. The final structures were analysed using AutoDock 4.2 software.[13]

ESR analysis

Sample preparation: Spin-labeled phosphatidylcholine (n-PCSL) were added to the lipid mixture (1% wt %/wt on the total lipid) by mixing appropriate amounts of a spin-label solution in ethanol (1 mg/mL) with the lipid organic mixture. A thin lipid film was produced by evaporating the solvents with dry nitrogen gas and final traces of solvents were removed by subjecting the sample to

vacuum desiccation for at least 3h. The samples were then hydrated with 30 μL of 10 mM phosphate buffer at pH = 7.4 and repeatedly vortexed, obtaining a MLV suspension. This suspension was transferred into a 25μL glass capillary and immediately sealed. Samples containing the peptide were prepared in a similar manner, except that the lipid film was hydrated directly with the peptide solution phosphate buffer at pH = 7.4 (peptide concentration of 2 mg/ml).

Spectra acquisition. Electron spin resonance spectra of lipid and lipid/peptide samples were recorded on a 9-GHz Bruker Elexys E-500 spectrometer (Bruker, Rheinstetten, Germany). Capillaries containing the samples were placed in a standard 4-mm quartz sample tube and the temperature was maintained constant during the measurement. The instrumental settings were as follows: sweep width 120 G, resolution 1.024 points, modulation frequency 100 kHz, modulation amplitude 1.0 G, time constant 20.5 ms, incident power 5.0 mW. Several scans, typically 16, were accumulated to improve the signal-to-noise ratio. Values of the outer hyperfine splitting, $2A_{max}$, were determined by measuring the difference between the low-field maximum and the high-field minimum.[14, 15] The main source of error on the $2A_{max}$ value is the uncertainty in composition of samples prepared by mixing few microliters of mother solutions. For this reason, reproducibility of $2A_{max}$ determination was estimated by evaluating its value for selected independently prepared samples with the same nominal composition. It was found to be § 0.2–0.3 G. The spin-labelled n-PCSL, with the nitroxide group at different positions, n, in the sn-2 acylchain were purchased from Avanti Polar Lipids (Birmingham, AL, USA). The spin-labels were stored at -20°C in ethanol solutions at a concentration of 1 mg/ml.

Molecular dynamics: computational Protocol

System parameterization. The C8 starting structure was obtained from the NMR experiments described above and then parameterized using the ff99SBildn, force fields of Amber14 suite. (http://ambermd.org) Six bilayers with different DOPC/DOPG molar ratio using charmm-gui.org (http://charmm-gui.org) and parameterized with lipid11 force field (http://ambermd.org) were built: i) pure DOPC, ii) DOPC/DOPG 90:10, iii) 60:40, iv) 40:60, v) 10:90 and vi) pure DOPG.

Systems setup and MD simulations. All the simulations were carried out using the NAMD 2.9 software[16] (http://www.ks.uiuc.edu/Research/namd/) and TIP3P as water solvation model. Each C8-bilayer system, was solvated using the vmd autoionize plugin[17] (http://www.ks.uiuc.edu/Research/vmd/).

Generation of the Peptide-Membrane complexes and FMD simulations.

The initial distance between the centre of mass of the peptide and the centre of mass of the membrane was set equal to 35 Å. The obtained systems were submitted to a relaxation protocol as described in the System Setup and MD simulations section. Finally, a production phase was conducted for 10 ns in the NPT ensemble with a target pressure equal to 1.01325 bar, a time-step of 2 fs, and using the RATTLE algorithm for the hydrogen atoms. The temperature was retained at 300 K using the Langevin thermostat. During the 10 ns of production phase, the position of the peptides relative to the membrane was restrained.[18] The conformational space to explore was reduced using a funnel-restrained potential. Using the funnel potential during the simulation, as the peptide reaches the edge of the funnel, a repulsive bias is applied to the system, disfavouring it from visiting regions outside the funnel. Finally, the frames where the system feels the external potential were not considered for the statistical analysis of the simulations.

Analysis of the distance and the number of contacts between the C8 peptide and the membrane. We analysed the distance and number of contacts formed between the C8 peptide and the polar head of both DOPC and DOPG phospholipids during the six different FMD simulations. The analysis was performed using the g_mindist tool of Gromacs V. 4.6.7[19] with a contacts cut-off of 4 Å. The minimum distance reported in figure 4C was calculated between Cα atom of Val5 in C8 and the atoms of the polar heads of both DOPC and DOPG phospholipids. From this analysis we have defined two parameters to classify the binding states of the peptide.

Cluster analysis.. The clustering was carried out using the g_cluster tool with the GROMOS algorithm of Gromacs V. 4.6.7.[19] The clustering was performed on the RMSD (Root Mean Square Deviation) value of the Cα atoms of the whole peptide core (1-8 aa) using a cut-off of 2 Å.

Membrane thickness calculation. To quantify the membrane thickness, we computed the local 1-D electron density profile in pure DOPC (i.e. 100:0 DOPC/DOPG) and DOPC/DOPG 90:10 membranes, projected along the bilayer normal. The density profile computations were performed with the VMD plugin Density Profile Tool (http://multiscalelab.org/utilities/Density ProfileT)

Confocal Microscope Imaging

Multilamellar lipid vesicle preparation. The multilamellar lipid vesicles (MLVs) of DOPC, DOPG and DOPC/DOPG (90:10, 70:30, 30:70, and 10:90 M/M) were prepared by mixing appropriate amounts of lipids, dissolved in dichloromethane/methanol mixture (25 mM lipid concentration), in a round-bottom test tube. The total weight of the lipid for each sample was 1.0 mg. MLVs were prepared from lipid DOPC and DOPG solutions that were desiccated, dried

overnight and hydrated in a 10 mM phosphate buffer at pH 7.4. MLVs were prepared in six different lipid compositions: DOPC only, DOPG only, DOPC/DOPG 90:10 M/M, DOPC/DOPG 70:30 M/M, DOPC/DOPG 30:70 M/M and DOPC/DOPG 10:90 M/M. MLVs, in the presence of NBD-labelled C8, NBD-labelled C6a and NBD-labelled C6b peptides, were prepared by adding during their formation, the labelled peptides at a concentration of 0.5 mM (lipid to peptide 50:1 M/M). Lipid solutions in the presence or absence of labelled peptides were used for microscopy analysis.[20]

Cellular vesicle preparation. *HeLa* cells were routinely grown at 37°C in a humidified atmosphere with 5% CO2 in DMEM 10% FBS supplemented with 4.5 g/l D-glucose, 1mM Na-pyruvate, 2mM L-glutamine. 5 x 106 actively growing cells were seeded in T75 tissue culture flasks and processed for blebs isolation after 24 hours.

To produce blebs, we replaced DMEM with a Blebbing Active Solution (20mM CaCl2, 10mM Hepes, 150mM NaCl, 2mM DTT, 25mM HCOH) and incubated flasks at 37°C, 60 rpm for 2h30'. After this step, we transferred the supernatant into a 50 mL falcon and left to settle the blebs for 1h in ice.

A total of 10 µL of each solution, in the presence or absence of peptides, was taken and spotted onto a cover slip. Images were acquired as previously described [21, 22] on a laser scanning confocal microscope (LSM 510; Carl Zeiss MicroImaging) equipped with a plan Apo 63X, NA 1.4 oil immersion objective lens. For each field, both fluorescent and transmitted light images were acquired on separate photomultipliers and were analysed with Zeiss LSM 510 4.0 SP2 software. In samples in which different z-planes were distinguishable, a z-stack acquisition mode was performed to focus a single z-plane, as published previously.[23]

Microscopy imaging. A total of 10 µL of each solution, in the presence or absence of NBD-labelled C8, NBD-labelled C6a and NBD-labelled C6b peptides was taken and spotted onto a cover slip. Images were acquired as previously described[21, 22] on a laser scanning confocal microscope (LSM 510; Carl Zeiss MicroImaging) equipped with a plan Apo 63X, NA 1.4 oil immersion objective lens. For each field, both fluorescent and transmitted light images were acquired on separate photomultipliers and were analysed with Zeiss LSM 510 4.0 SP2 software. In samples in which different z-planes were distinguishable, a z-stack acquisition mode was performed to focus a single z-plane, as published previously.[23]

References

1. Scrima, M.; Di Marino, S.; Grimaldi, M.; Campana, F.; Vitiello, G.; Piotto, S. P.; D'Errico, G.; D'Ursi, A. M. Structural features of the C8 antiviral peptide in a membrane-mimicking environment. *Biochim. Biophys. Acta* **2014,** 1838, 1010-8.
2. Dufau, I.; Mazarguil, H. Design of a fluorescent amino acid derivative usable in peptide synthesis. *Tetrahedron Letter.* **2000,** 41, 6063-6066.
3. Zerbe, O. BioNMR in drug research methods and principles in medicinal chemistry. **2003**.
4. Whitmore, L.; Wallace, B. A. DICHROWEB, an online server for protein secondary structure analyses from circular dichroism spectroscopic data. *Nucleic Acids Res.* **2004,** 32, W668-73.
5. Piantini, U.; Sorensen, O.; Ernst, R. R. Multiple quantum filters for elucidating NMR coupling networks. *J. Am. Chem. Soc.* **1982,** 104, 6800-6801.
6. Bax, A.; Davis, D. G. MLEV-17-based two-dimensional homonuclear magnetization transfer spectroscopy. *J. Magn. Reson.* **1985,** 65, 355-360.
7. Jeener, J.; Meier, B.; Bachmann, P.; Ernst, R. Investigation of exchange processes by two-dimensional NMR spectroscopy. *J. Chem. Physics* **1979,** 71, 4546-4553.
8. Piotto, M.; Saudek, V.; Sklenář, V. Gradient-tailored excitation for single-quantum NMR spectroscopy of aqueous solutions. *J. Biom. NMR* **1992,** 2, 661-665.
9. Goddard, T.; Kneller, D. SPARKY 3. *University of California, San Francisco* **2004**.
10. Güntert, P.; Mumenthaler, C.; Wüthrich, K. Torsion angle dynamics for NMR structure calculation with the new program D1. *J. Mol. Biol.* **1997,** 273, 283-298.
11. Pearlman, D. A.; Case, D. A.; Caldwell, J. W.; Ross, W. S.; Cheatham, T. E.; DeBolt, S.; Ferguson, D.; Seibel, G.; Kollman, P. AMBER, a package of computer programs for applying

molecular mechanics, normal mode analysis, molecular dynamics and free energy calculations to simulate the structural and energetic properties of molecules. *Com. Physics Comm.* **1995,** 91, 1-41.

12. Case, D. A.; Pearlman, D. A.; Caldwell, J. W.; Cheatham III, T. E.; Wang, J.; Ross, W. S.; Simmerling, C.; Darden, T.; Merz, K. M.; Stanton, R. V. AMBER 7. *University of California, San Francisco* **2002**.

13. Rizvi, S. M.; Shakil, S.; Haneef, M. A simple click by click protocol to perform docking: AutoDock 4.2 made easy for non-bioinformaticians. *EXCLI J.* **2013,** 12, 831-57.

14. Marsh, D.; Horvath, L. I. Structure, dynamics and composition of the lipid-protein interface. Perspectives from spin-labelling. *Biochim Biophys Acta* **1998,** 1376, 267-96.

15. Schorn, K.; Marsh, D. Lipid mixing in dimyristoyl phosphatidylcholine-dimyristoyl glycerol dispersions: spin label ESR studies. *Biochim Biophys Acta* **1997,** 1323, 57-64.

16. Kalé, L.; Skeel, R.; Bhandarkar, M.; Brunner, R.; Gursoy, A.; Krawetz, N.; Phillips, J.; Shinozaki, A.; Varadarajan, K.; Schulten, K. NAMD2: greater scalability for parallel molecular dynamics. *Journal of Computational Physics* **1999,** 151, 283-312.

17. Humphrey, W.; Dalke, A.; Schulten, K. VMD: visual molecular dynamics. *Journal of molecular graphics* **1996,** 14, 33-38.

18. Limongelli, V.; Bonomi, M.; Parrinello, M. Funnel metadynamics as accurate binding free-energy method. *Proceedings of the National Academy of Sciences* **2013,** 110, 6358-6363.

19. Spoel, D.; Lindahl, E.; Hess, B.; Buuren, A.; Apol, E.; Meulenhoff, P.; Tieleman, D.; Sijbers, A.; Feenstra, K.; Drunen, R. Gromacs User Manual version 4.6. 7, 2014. In.

20. Kaiser, E.; Colescott, R.; Bossinger, C.; Cook, P. Color test for detection of free terminal amino groups in the solid-phase synthesis of peptides. *Anal. Biochem.* **1970,** 34, 595-598.

21. Amodio, G.; Sasso, E.; D'Ambrosio, C.; Scaloni, A.; Moltedo, O.; Franceschelli, S.; Zambrano, N.; Remondelli, P. Identification of a microRNA (miR-663a) induced by ER stress and its target gene PLOD3 by a combined microRNome and proteome approach. *Cell biology and toxicology* **2016,** 32, 285-303.

22. Ranieri, R.; Ciaglia, E.; Amodio, G.; Picardi, P.; Proto, M. C.; Gazzerro, P.; Laezza, C.; Remondelli, P.; Bifulco, M.; Pisanti, S. N6-isopentenyladenosine dual targeting of AMPK and Rab7 prenylation inhibits melanoma growth through the impairment of autophagic flux. *Cell Death Differ* **2018,** 25, 353-367.

23. Fasano, D.; Parisi, S.; Pierantoni, G. M.; De Rosa, A.; Picillo, M.; Amodio, G.; Pellecchia, M. T.; Barone, P.; Moltedo, O.; Bonifati, V.; De Michele, G.; Nitsch, L.; Remondelli, P.; Criscuolo, C.; Paladino, S. Alteration of endosomal trafficking is associated with early-onset parkinsonism caused by SYNJ1 mutations. *Cell Death Dis* **2018,** 9, 385.